

**ornl**

**OAK RIDGE  
NATIONAL  
LABORATORY**

**MARTIN MARIETTA**



3 4456 0146454 5

**ORNL/TM-9814**

**Effects of  
Directed and Kinetic Energy Weapons  
on Spacecraft**

**A. P. Fraas**

OAK RIDGE NATIONAL LABORATORY

CENTRAL RESEARCH LIBRARY

CIRCULATION SECTION

4500N ROOM 175

**LIBRARY LOAN COPY**

DO NOT TRANSFER TO ANOTHER PERSON

If you wish someone else to see this  
report, send in name with report and  
the library will arrange a loan.

OCT 1989 3 4 77

OPERATED BY  
MARTIN MARIETTA ENERGY SYSTEMS, INC.  
FOR THE UNITED STATES  
DEPARTMENT OF ENERGY

Printed in the United States of America. Available from  
National Technical Information Service  
U.S. Department of Commerce  
5285 Port Royal Road, Springfield, Virginia 22161  
NTIS price codes—Printed Copy: A05 Microfiche A01

This report was prepared as an account of work sponsored by an agency of the United States Government. Neither the United States Government nor any agency thereof, nor any of their employees, makes any warranty, express or implied, or assumes any legal liability or responsibility for the accuracy, completeness, or usefulness of any information, apparatus, product, or process disclosed, or represents that its use would not infringe privately owned rights. Reference herein to any specific commercial product, process, or service by trade name, trademark, manufacturer, or otherwise, does not necessarily constitute or imply its endorsement, recommendation, or favoring by the United States Government or any agency thereof. The views and opinions of authors expressed herein do not necessarily state or reflect those of the United States Government or any agency thereof.

Engineering Technology Division

EFFECTS OF DIRECTED AND KINETIC ENERGY WEAPONS  
ON SPACECRAFT

A. P. Fraas  
Consultant

Manuscript Completed — April 1986  
Date Published — December 1986

**NOTICE** This document contains information of a preliminary nature.  
It is subject to revision or correction and therefore does not represent a  
final report.

Prepared by the  
OAK RIDGE NATIONAL LABORATORY  
Oak Ridge, Tennessee 37831  
MARTIN MARIETTA ENERGY SYSTEMS, INC.  
for the  
U.S. Department of Energy  
under Contract No. DE-AC05-84OR21400



3 4456 0146454 5



## CONTENTS

	<u>Page</u>
ABSTRACT .....	1
1. INTRODUCTION .....	1
2. BACKGROUND OF EXPERIENCE .....	3
3. TYPES OF ENERGY BEAMS AND THEIR EFFECTS .....	7
3.1 Neutral Beams .....	7
3.2 Electron Beams .....	7
3.3 Laser Beams .....	9
3.4 X Rays .....	12
4. DAMAGE MODES .....	21
4.1 Surface Heating .....	21
4.2 Temperature Distribution in Short Bursts .....	29
4.3 Explosive Vaporization .....	35
4.4 Thermal Stresses .....	46
4.5 Overall View of Failure Modes .....	47
5. SURVEY OF SOME TYPICAL CASES .....	53
5.1 Relations Between Pulse Energy, Duration, and Power ....	53
5.2 Swarms of Birdshot .....	57
5.3 Shielding Spacecraft from Hostile Action .....	62
REFERENCES .....	67
Appendix A. TEMPERATURE DISTRIBUTIONS IN PLATES WITH SURFACES HEATED BY SHORT BURSTS OF RADIANT ENERGY .....	71
Appendix B. BLAST EFFECTS FROM RAPID VAPORIZATION FROM A SURFACE .....	73



EFFECTS OF DIRECTED AND KINETIC ENERGY WEAPONS  
ON SPACECRAFT

A. P. Fraas

ABSTRACT

The characteristics of the various directed energy beams are reviewed, and their damaging effects on typical materials are examined for a wide range of energy pulse intensities and durations. Representative cases are surveyed, and charts are presented to indicate regions in which damage to spacecraft structures, particularly radiators for power plants, would be likely. The effects of kinetic energy weapons, such as bird-shot, are similarly examined. The charts are then applied to evaluate the effectiveness of various measures designed to reduce the vulnerability of spacecraft components, particularly nuclear electric power plants.

---

1. INTRODUCTION

A major yet subtle set of considerations in the design of power plants for military spacecraft is concerned with the reduction of their vulnerability to weapons such as lasers and particle beams. This memorandum was prepared to give perspective to these problems and provide data and charts that will help in estimating the vulnerability to typical weapons of the various concepts and designs under consideration. The presentation was designed for use by engineers having relatively little background in the many specialized disciplines involved; hence, rough approximations are employed to simplify the presentation.



## 2. BACKGROUND OF EXPERIENCE

In attempting to visualize the effects of intense beams of radiation on spacecraft structures, it is helpful to look first at some of the background of experience that is available. The basic concept is not as new as it may seem. About 200 B.C. catastrophic damage to military equipment by radiant energy was experienced by the Romans when the Greeks at Syracuse followed Archimedes' suggestion and used their polished shields to form a multifaceted mirror to concentrate the rays of the sun on the sails of attacking Roman ships and set them on fire. Leonardo da Vinci tried to build a large parabolic mirror with many facets of silvered glass for the defense of Milan. Apparently, however, he was frustrated by difficulties in getting a sufficiently high degree of stiffness and dimensional stability in the support structure to give a parabolic surface that would yield and maintain a sharp focus. These same problems have plagued efforts to get large, lightweight, parabolic mirrors for focusing sunlight on small boilers for Rankine cycle power plants for spacecraft in spite of tens of millions of dollars spent by both the U.S. Air Force and the National Aeronautics and Space Administration (NASA) between 1958 and 1975. Although progress has been slow, recent U.S. developments on mirrors for concentrating solar energy for space power plants look promising.<sup>1</sup> A weapons system employing large mirrors to concentrate solar energy into beams for use against spacecraft is not likely, however, because the solar disc subtends an angle of  $1/2^\circ$  so that optical considerations yield a divergence angle of at least  $1/2^\circ$  for any beam concentrated by a concave mirror.

The advent of the nuclear age introduced a new set of problems involving severe radiation heating. The targets in particle accelerators, such as cyclotrons, were melted by the intense energy input from the beams; this led to water cooling of the targets. Even more-severe surface heating problems have been experienced in the development of thermonuclear reactors.<sup>2</sup> Figure 1 shows the surface melting experienced with a water-cooled copper target used in the development of neutral beams designed to ignite the plasma in thermonuclear experimental



Fig. 1. Photograph of a 4-mm-thick, water-cooled copper target employed in ORNL tests of neutral beam injectors. The energy per pulse was typically  $700 \text{ J/cm}^2$  with pulse durations of 0.05 s. The diameter of the melted zone in the center is  $\sim 1.5 \text{ cm}$  while that of the heavily fissured region around it is  $\sim 3 \text{ cm}$ . *Source:* A. P. Fraas and A. S. Thompson, *ORNL Fusion Power Demonstration Study: Fluid Flow, Heat Transfer, and Stress Analysis Considerations in the Design of Blankets for Thermonuclear Reactors*, ORNL/TM-5960, Union Carbide Corp. Nuclear Div., Oak Ridge Natl. Lab., February 1978, p. 51.

machines. Note that the bulk of the energy in the beam used on the target in Fig. 1 was in the form of 30-keV hydrogen ions whose energy was absorbed essentially at the surface, their penetration being only a tiny fraction of a millimeter. At this energy level even electrons are not very penetrating — still a small fraction of a millimeter. As will be discussed later, at higher energies electrons are more penetrating so that only a portion of the energy in a beam may be absorbed very close to the surface. Small, intense beams of relatively low-energy electrons are used in welding and for cutting complex shapes in difficult-to-machine metals and ceramics by the fairly widely used Eloxing process.<sup>3</sup>

Runaway electrons have been a major source of damage in thermonuclear experiments with Tokamaks, in some cases melting holes through the wall of the toroidal shell surrounding the plasma [e.g., in the French TFR and the Massachusetts Institute of Technology (MIT) Alcator]; in others they have melted limiters made of tungsten or molybdenum (see Fig. 2). (A limiter is a sharp-edged orifice having an aperture a bit smaller in diameter than the minor diameter of the toroidal shell so that electrons or ions orbiting out of the plasma will strike the limiter before reaching and melting a hole in the vacuum wall.) More details on these problems are presented in Ref. 2.

High-energy laser beams have been used for welding metals and for machining metal and ceramic parts.<sup>4,5</sup> Another pertinent area of experience, laser-fusion, has been directed toward the ignition of a thermonuclear reaction by concentrating a very short burst of energy in a laser beam on a frozen pellet of deuterium and tritium. To ignite a pellet roughly 2 mm in diameter will require that the laser beam energy be  $\sim 10^5$  J in a burst time of  $\sim 10^{-10}$  s. The laser beam energy does not heat the core of the pellet directly but, rather, vaporizes the surface layer of the pellet so rapidly that the reaction force from the exploding outer layers implodes, acting to compress and, thus, heat the core of the pellet. This compression-ignition process is analogous to that in a diesel engine, but the pressure and temperature regime required for deuterium-tritium ignition is vastly higher — on the order of 2000 Mbar and  $10^8$  K.<sup>6</sup>



Fig. 2. Photograph of damage to an ORMAK limiter made of tungsten laminations, each 3 mm thick. *Source:* A. P. Fraas and A. S. Thompson, *ORNL Fusion Power Demonstration Study: Fluid Flow, Heat Transfer, and Stress Analysis Considerations in the Design of Blankets for Thermonuclear Reactors*, ORNL/TM-5960, Union Carbide Corp. Nuclear Div., Oak Ridge Natl. Lab., February 1978, p. 42.

### 3. TYPES OF ENERGY BEAMS AND THEIR EFFECTS

#### 3.1 Neutral Beams

Intense ion beams were first developed for use in cyclotrons, an application that required a relatively low beam current. Vastly higher current beams were developed for the Calutrons employed for the separation of  $^{235}\text{U}$  and  $^{238}\text{U}$  during the Manhattan Project. Further developments requiring even higher currents have included ion jets for spacecraft propulsion and beams designed to ignite the plasma in thermonuclear reactor experiments. High-current beams tend to diverge rapidly because the ions have the same electrical charge and, therefore, repel each other. This effect can be largely eliminated by neutralizing the charge on the ions after they have been accelerated and collimated with electrostatic and magnetic fields; some neutralization systems have yielded neutral beams with remarkably little divergence. The energy efficiency of the systems for producing these neutral beams falls off with both the energy of the ions produced and with the degree of collimation of the final beam. Essentially all of the energy in beams of this type acts to heat any surface they strike with virtually no losses as a consequence of reflection by either the surface or the vapor layer evolved by heating the surface.

#### 3.2 Electron Beams

Electron beams are the basis for the cathode ray tubes that have made modern television possible. As mentioned previously, they are also employed for machining and welding, as well as for other less widespread applications. As shown in Fig. 3, the penetration of electron beams increases rapidly with their energy. Although they are not subject to appreciable reflection from a surface, they are not well suited for use as weapons against spacecraft because there is no way to eliminate the electrical charge effects cited above for ion beams; thus, the high degree of collimation required for a long-range space weapon cannot be

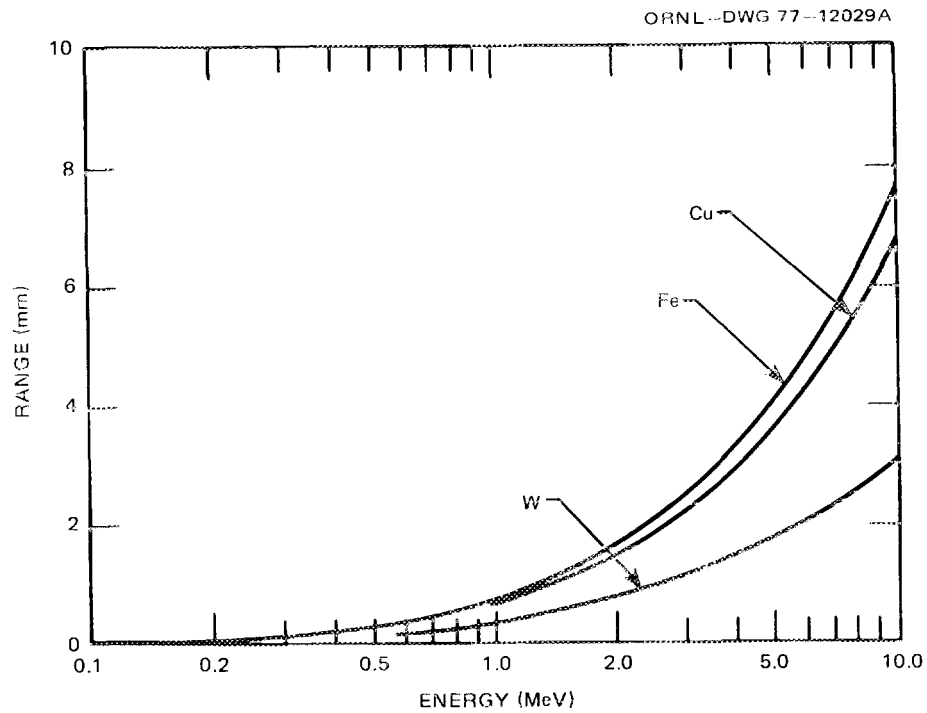


Fig. 3. Range of electron penetration in typical structural materials as a function of the energy of the incident electron. Source: M. Berger and S. M. Seltzer, *Tables of Energy Losses and Ranges of Electrons and Positrons*, NASA SP-3012, National Aeronautics and Space Administration, Washington, D.C., 1964, p. 37.

achieved. Long-range exoatmospheric beams of electrons and ions are also bent by the earth's magnetic field.

### 3.3 Laser Beams

The broad spectrum of electromagnetic radiation shown diagrammatically in Fig. 4 offers possibilities for long-range, directed-energy weapons, particularly lasers operating in the region from soft X rays to the infrared with wavelengths from  $\sim 0.001$  to  $10 \mu\text{m}$ . Although longer wavelengths to produce microwave heating might be considered, these beams are less suitable for long-range weapons because their angular divergence increases approximately in proportion to the wavelength. At the other end of the spectrum, radiation in the wavelength region below  $1 \mu\text{m}$  does not appear suitable for a weapon because of the physical difficulties of creating coherent beams at progressively shorter wavelengths.

The energy efficiency for the generation of laser beams varies widely, ranging from  $<1\%$  to as much as  $30\%$ , depending on the type of laser. Some lasers are suited to the production of a continuous beam; others operate in a pulsed mode with pulses as short as  $10 \text{ ps}$ . As will be discussed in Sect. 4, there are important advantages to the use of very short pulses (e.g.,  $<100 \text{ ns}$ ), but the efficiency of lasers giving these short pulses tends to be low.

The energy of a laser beam may be absorbed in the material that it strikes, or much of it may be reflected, depending on the reflectivity of the surface. Figure 5 shows that the reflectivity for some typical surfaces varies widely both with the wavelength and from one material to another. Thus, a flash plating of polished silver would reflect most of the energy in an incident laser beam over a wide range of wavelengths. The surface need not necessarily be polished; a white surface might also reflect the bulk of the incident radiation by diffuse reflection even if its specular reflectivity is poor. For example, the upper surface of the fuselage of passenger aircraft is commonly painted white because this gives much less heat absorption than bare polished aluminum on a

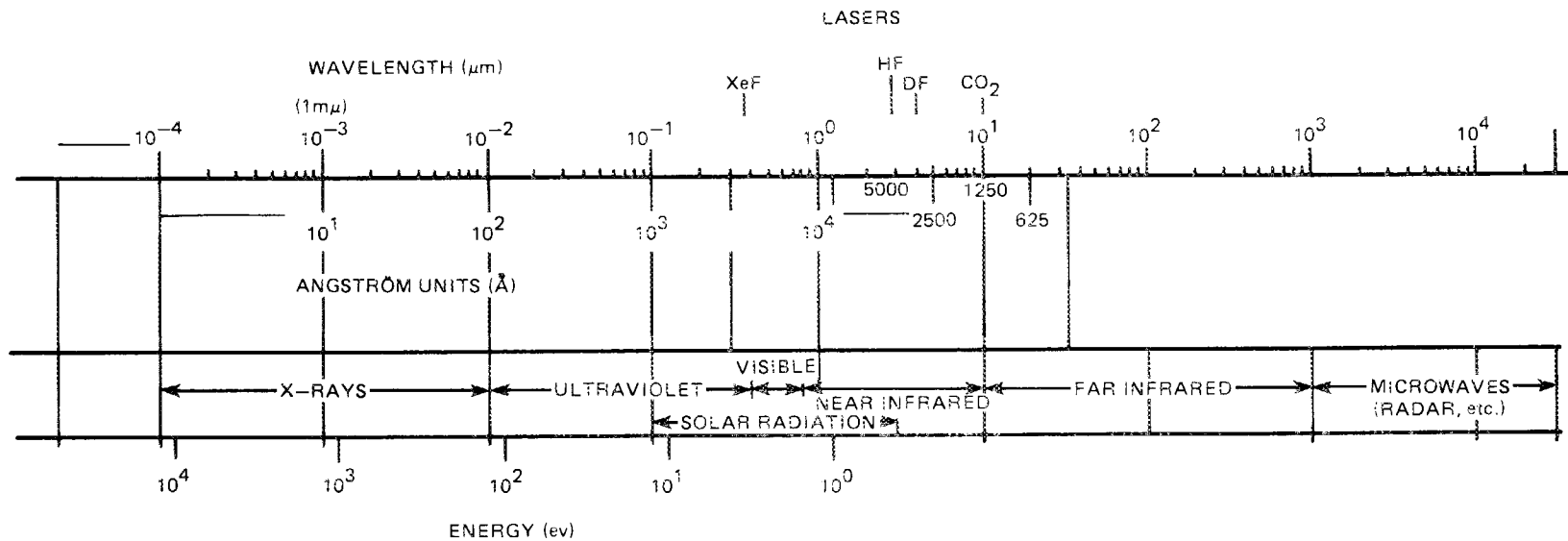


Fig. 4. The electromagnetic spectrum, compared with the wavelengths for typical lasers and particle size scales.

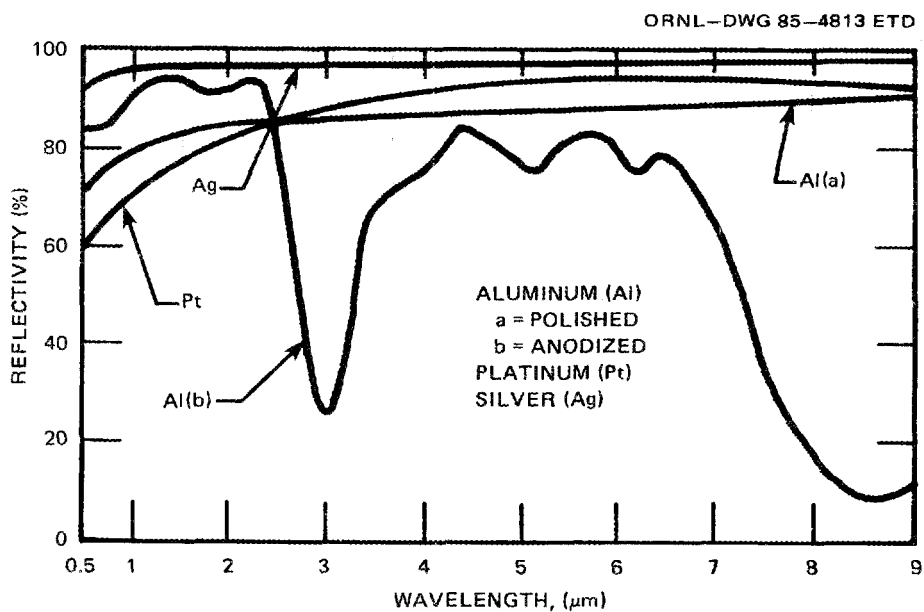


Fig. 5. Variation of reflectivity with wavelength for typical metals. Source: *Handbook of Chemistry and Physics*, 40th ed., CRC Press, Cleveland, 1959, p. 2948.

bright summer day and, thus, greatly reduces the air-conditioning load. Unfortunately, most handbook data on reflectivity are for specular reflection only — the total fraction of the incident light that would be reflected might be much higher. For example, although the specular reflectivity of painted surfaces is poor, a glossy white enamel may reflect 85% of incident sunlight via diffuse reflection, whereas Marine Corps green may reflect only 4%.<sup>7</sup> Data for the reflectivity of typical materials for the full range of wavelengths of light are sometimes hard to find. Table 1 gives a representative set.

Absorbed energy may be re-emitted as thermal radiation. Figure 6 gives a comprehensive chart for the radiation flux from an ideal black body having an emissivity of 1.0; Table 2 gives data for the emissivity of surfaces likely to be of interest for spacecraft.

### 3.4 X Rays

Although low-energy photons having wavelengths in the visible light range penetrate a little into the crystal lattice of metals, the distance is very short. For example, the attenuation length in iron is only about 10 lattice spacings.<sup>8</sup> However, for much shorter wavelengths (i.e., in the X-ray region) the attenuation length becomes substantial. Because soft X rays are not reflected (except at low angles of incidence) and penetrate an appreciable distance beneath the surface, they pose a quite different set of problems from either particle beams or lasers. The depth of penetration depends on both the wavelength and the material of the surface, the mass absorption coefficient increasing with the atomic weight (see data in Table 3 from Ref. 9). Data from Table 3 were used in the calculations of Table 4 to determine the fraction of the energy absorbed in the first millimeter of a target as a function of the wavelength for several typical metals. These results have been plotted in Fig. 7. Very little energy from a 0.005- $\mu\text{m}$  X-ray beam would be absorbed in the wall of a spacecraft if it were made of a 1-mm-thick sheet of beryllium; most of the energy from the same beam, however, would be absorbed in a 1-mm-thick steel wall. The resulting instantaneous temperature rise in the wall from a short pulse of 50 J/cm<sup>2</sup> is shown in Fig. 8.

Table 1. Reflection of light by metals<sup>a</sup>

Material	Wavelength ( $\mu\text{m}$ )								
	0.251	0.357	0.500	8.000	1.000	2.000	4.000	9.000	12.000
Aluminum					71.0	82.0	92.0		98.0
Antimony					55.0	60.0	68.0	72.0	
Bronze (68 Cu, 32 Sn)	30.0		63.0		70.0	80.0	88.0	93.0	
Cadmium					72.0	87.0	96.0		99.0
Cobalt					67.0	72.0	81.0		97.0
Copper (commercial)	25.9	27.3	43.7	88.6	90.1	95.5	97.3	98.4	
Gold (electrolytic)	38.8	27.9	47.0	94.9		96.8	96.9	98.0	
Graphite			22.0	25.0	27.0	35.0	48.0		
Iridium					78.0	87.0	94.0		96.0
Iron			55.0		65.0	78.0	89.0	94.0	
Magnalium (Mach's)	67.0	81.2	83.3	84.3	84.1	86.7	88.7	90.6	
Magnesium			72.0		74.0	77.0	83.0	93.0	
Mercury-backed glass			70.9						
Molybdenum			46.0	52.0	58.0	82.0	90.0		95.0
Nickel (electrolytic)	37.8	48.8	60.8	69.6	72.0	83.5	91.1	95.6	
Palladium					72.0	81.0	88.0		97.0
Platinum (electrolytic)	33.8	43.4	58.4	70.3	72.9	80.6	91.5	95.4	
Rhodium			76.0	81.0	84.0	91.0	92.0		
Silicon			34.0	29.0	28.0	28.0	28.0		
Silver (chemically deposited)	34.1	74.5	91.3	96.8	97.0	97.8	98.5	98.7	
Silver-backed glass			86.6						
Speculum metal	29.9	51.0	63.2		70.5	80.4	88.5	92.2	
Steel	32.9	45.0	54.8	58.0	63.1	76.7	87.8	92.9	
Stellite					68.9	74.7	82.5	88.0	
Tantalum			38.0	64.0	78.0	90.0	93.0		95.0
Tellurium				48.0	50.0	52.0	57.0		
Tin					54.0	61.0	72.0		85.0
Tungsten			49.0		62.0	85.0	93.0	95.0	
Vanadium			57.0	60.0	61.0	69.0	79.0		
Zinc					80.0	92.0	97.0		99.0

<sup>a</sup>The table gives the percentage of normally incident light that is reflected by the polished surface of various metals as a function of the wavelength of the light.

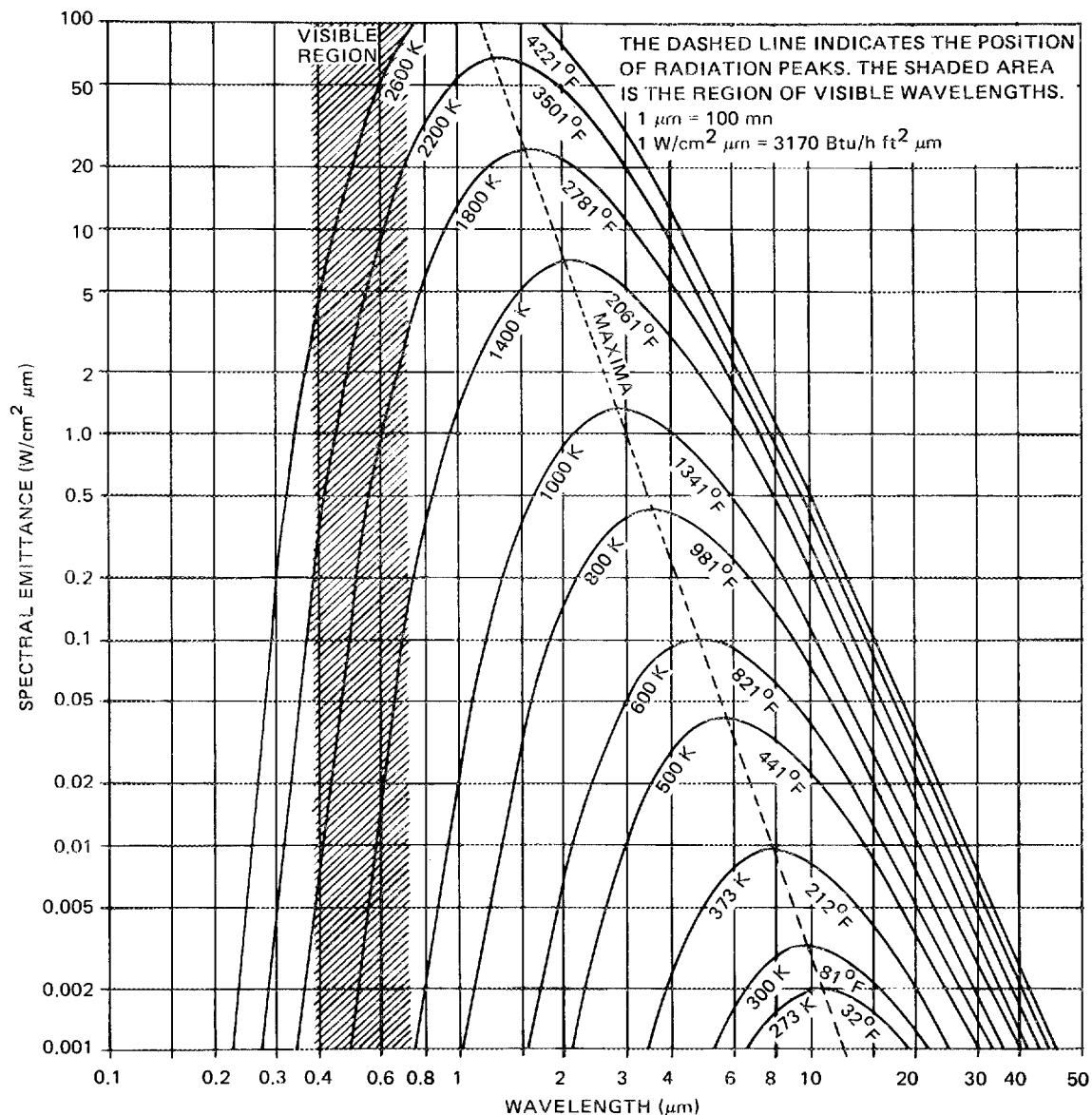


Fig. 6. Black-body spectral intensities for source temperatures between 273 and 2600 K. Source: R. E. Bolz and G. L. Tuve, eds., *Handbook of Tables for Applied Engineering Science*, 2d ed., CRC Press, Cleveland, 1973, p. 208.

Table 2. Emissivities for typical surfaces

Surface	Emissivity at various temperatures in °F (%)										
	-250	100	125	300	500	750	1000	1500	2000	2500	5000
<i>Metals</i>											
Aluminum, polished, 98% pure	4		4	5		8		17		26	
Aluminum, oxidized	20		21	23		33					
Copper, polished				2		4		6			
Copper, black oxide	92		90	83		77					
Chromium, polished sheet	8		14	17		27		37		.43	
Gold, electrolytic, polished	2		2	2		3		62			
Iron and steel, pure polished iron	6		6	8		12		22		35	
Iron and steel, cast iron, polished	21		21	21		21					
Iron and steel, polished steel	7		8	10		14		23		37	
Iron and steel, rough steel plate	94		95	97		98					
Iron and steel, cast iron, oxidized	58		62	66		75					
Iron and steel, matt wrought iron, oxidized	95		95	95							
Iron and steel, oxidized steel, after long heating at dull red	85		90	93		96					
Lead, pure, polished	5		6	8							
Magnesium, polished	7		10	13		18		23		26	
Molybdenum, polished	6		6	8		11		18		43	
Nickel, electrolytic	4		5	6		10		16		28	
Platinum, pure polished	4		5	6		10		19		27	
Platinum, black	93		94	96		97		97		97	
Rhodium, polished	5		7	7		8		9		16	
Silicon, polished	72		72	72		72		72		72	
Silver, polished or deposited	1		2	2		3		3		4	
Tantalum, polished	6		7	7		7		9		25	
Tellurium, polished	22		33	39		45		48		51	
Tungsten, polished	2		2.5	3.5		7.5		15		35	
Vanadium, polished	8		12	17		23		31		39	
Zinc, pure polished	2		2	3		4		6		50	
Zinc, matt zinc	21		21	21							
Alloys, brass, polished	10		10	10							
Alloys, brass, oxidized	46		50	56		75					
Alloys, nichrome wire, bright	65		66	67		71		79			
Alloys, nichrome wire, oxidized	95		96	97		98					
Alloys, stellite (Cr, Mo, Co)	12		13	14		18		24		28	
<i>Pigments</i>											
Acetylene soot	97		99			99					99
Blue (Co <sub>2</sub> O <sub>3</sub> )	94		87			86					97
Red (Fe <sub>2</sub> O <sub>3</sub> )	91		96			70					59
Green (Cr <sub>2</sub> O <sub>3</sub> )	92		95			67					55
White (Al <sub>2</sub> O <sub>3</sub> )	94		98			79					12
White (Al <sub>2</sub> O <sub>3</sub> )								38	46	46	
White (ZrO <sub>2</sub> )	95		95			77					16

Table 3. Calculated mass absorption coefficients (cm<sup>2</sup>/g)  
for X-ray attenuation in typical elements<sup>a</sup>

Element	Energy (eV)														
	1000	600	400	200	100	60	40	20	10	6	4	2	1	0.6	0.4
	Wavelength [ $\lambda$ (Å)]														
	0.012	0.020	0.030	0.060	0.12	0.20	0.3	0.6	1.2	2.0	3.0	6.0	12	20	30
H	0.1240	0.1577	0.1870	0.2407	0.2926	0.3263	0.3498	0.3736	0.4069	0.4927	0.7375	3.142	22.32	101.6	340.7
Li	0.0540	0.0687	0.0814	0.1049	0.1277	0.1433	0.1563	0.1939	0.4258	1.362	4.181	31.92	249.0	1,120	3,649
Be	0.0554	0.0705	0.0835	0.1076	0.1314	0.1487	0.1660	0.2443	0.7978	3.058	9.851	76.19	586.1	2,576	8,118
C	0.0624	0.0794	0.0941	0.1215	0.1494	0.1741	0.2089	0.4494	2.280	9.765	32.10	246.2	1,821	7,522	21,549
O	0.0625	0.0795	0.0943	0.1220	0.1529	0.1897	0.2614	0.8649	5.550	24.57	80.71	601.9	4,135	14,957	
Mg	0.0616	0.0784	0.0933	0.1222	0.1654	0.2541	0.4822	2.615	19.05	83.93	267.6	1,775			
Al	0.0602	0.0767	0.0910	0.1201	0.1672	0.2740	0.5573	3.226	23.68	103.6	326.7	2,072			
Si	0.0623	0.0794	0.0945	0.1250	0.1788	0.3100	0.6652	4.028	29.74	129.6	406.2	2,507			
K	0.0607	0.0776	0.0929	0.1285	0.2267	0.5420	1.445	9.998	72.68	298.5	851.4				
Ca	0.0624	0.0798	0.0956	0.1338	0.2480	0.6261	1.713	11.98	86.38	348.8	954.4				
Ti	0.0575	0.0736	0.0885	0.1273	0.2612	0.7257	2.068	14.64	103.5	401.4					
Cr	0.0578	0.0741	0.0896	0.1330	0.3025	0.9100	2.669	18.98	130.7	481.7					
Fe	0.0584	0.0750	0.0911	0.1403	0.3533	1.134	3.395	24.10	160.8						
Ni	0.0599	0.0771	0.0943	0.1512	0.4198	1.420	4.311	30.41	195.4						
Cu	0.0573	0.0739	0.0907	0.1486	0.4323	1.495	4.561	32.02	201.4						
Mo	0.0556	0.0740	0.0972	0.2221	1.020	4.045	12.37	75.17							
Ag	0.0558	0.0755	0.1031	0.2695	1.353	5.500	16.51								
Sr	0.0542	0.0743	0.1040	0.2942	1.571	6.324	18.61								
Ta	0.0552	0.0858	0.1475	0.6326	3.797										
W	0.0552	0.0865	0.1504	0.6538	3.923										
Pt	0.0558	0.0903	0.1635	0.7484	4.464										
Au	0.0562	0.0917	0.1677	0.7770	4.623										
Hg	0.0562	0.0925	0.1709	0.8008	4.751										
Pb	0.0563	0.0944	0.1778	0.8507	5.010										

<sup>a</sup>Data selected from tables in J. W. Victoreen, "The Calculation of X-ray Mass Absorption Coefficients in Practice," *J. Appl. Phys.* 20, 1141-47 (December 1949).

Table 4. X-ray attenuation in metal walls

Wavelength (Å)	Energy (eV)	Metal density (g/cm <sup>3</sup> )							
		Be 1.80		Mg 1.74		Al 2.77		Fe 7.87	
		$\mu^a$	$F^b$	$\mu$	F	$\mu$	F	$\mu$	F
2.50	4.8	5.789	0.647	159.30	1.00	195.60	1.00		1.00
2.00	6.0	3.058	0.423	83.93	1.00	103.60	1.00		1.00
1.50	8.0	1.393	0.222	36.46	1.00	45.24	1.00	284.00	1.00
1.00	12.0	0.533	0.091	11.21	0.86	13.95	0.98	99.10	1.00
0.80	15.0	0.355	0.062	5.89	0.64	7.32	0.87	53.86	1.00
0.50	24.0	0.208	0.037	1.59	0.24	1.95	0.42	14.38	0.98
0.40	30.0	0.184	0.033	0.91	0.15	1.09	0.26	7.64	0.88
0.30	40.0	0.166	0.029	0.48	0.08	0.56	0.14	3.40	0.61
0.20	60.0	0.149	0.026	0.25	0.04	0.27	0.07	1.13	0.27
0.15	80.0	0.139	0.025	0.19	0.03	0.20	0.05	0.56	0.14
0.10	120.0	0.125	0.022	0.15	0.03	0.15	0.04	0.26	0.07

<sup>a</sup>Mass attenuation coefficient, cm<sup>2</sup>/g.

<sup>b</sup>Fraction of energy absorbed in first millimeter;  $F = 1 - e^{-0.1 \mu \rho}$ .

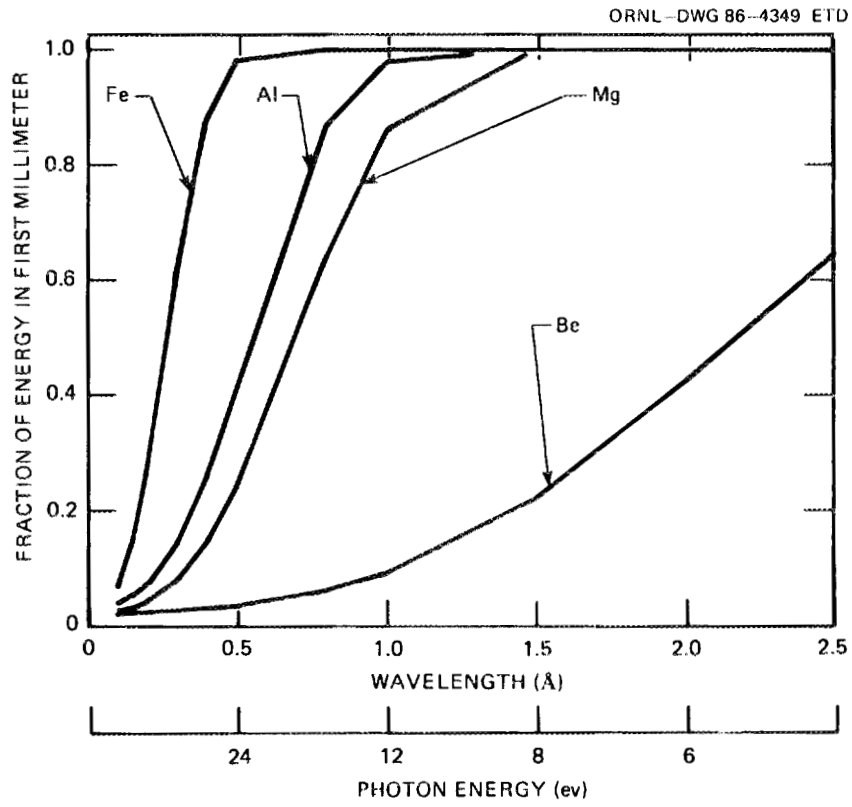


Fig. 7. X-ray energy absorbed in the first 1.0 mm as a function of wavelength for four metals (data from Table 4).

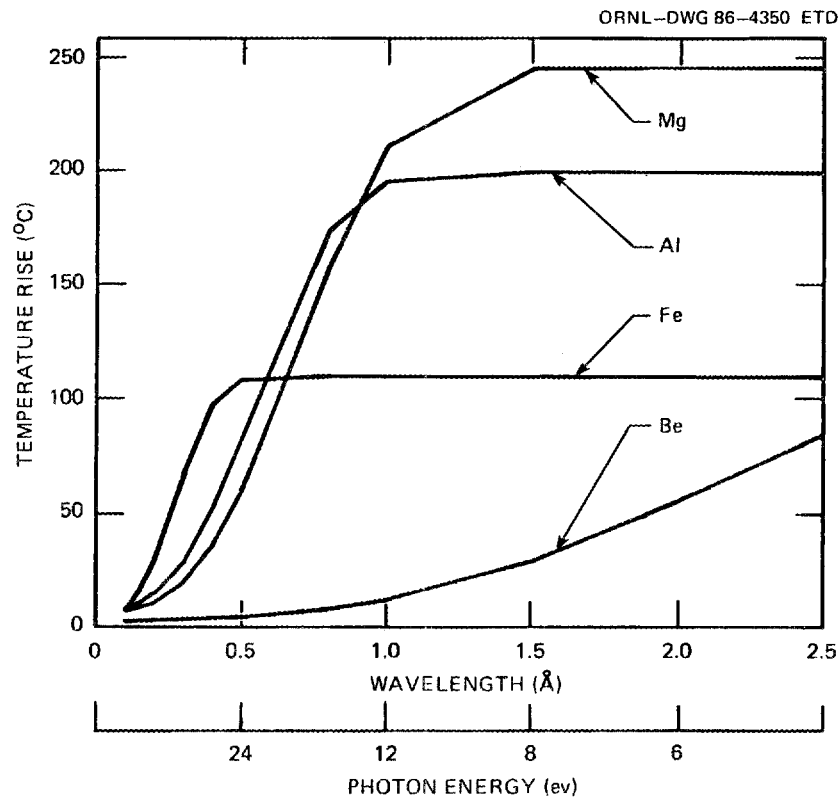


Fig. 8. Temperature rise in a 1.0-mm sheet for a  $50\text{-J/cm}^2$  burst of X rays as a function of wavelength for four different metals (data from Table 4). (The temperature rise is independent of the time required for the burst for times  $<1.0$  s.)



#### 4. DAMAGE MODES

The preceding overview indicates that a variety of radiant energy beams operating with a wide range of pulse energy densities and pulse durations might damage spacecraft structures. Types of damage include the overheating of temperature-sensitive materials, such as the semiconductors in solar cells; the heating of structural components until they weaken or melt; the explosive vaporization of a thin surface layer by subjecting it to a very short, intense burst of energy; and heating to impose severe thermal stress.

##### 4.1 Surface Heating

The damage mode most easily visualized and assessed is the surface heating produced by a continuous beam of relatively low intensity. Such a beam may heat an exposed surface until it melts or vaporizes unless it is sufficiently refractory so that it can operate at a temperature high enough to dissipate heat by thermal radiation at the same rate as it is absorbing energy from the beam. A first step in assessing the damaging effects of a beam weapon is to estimate the temperature rise in typical materials as a function of the amount of heat absorbed. Thus, the melting and boiling points, the latent heats of fusion and vaporization, and the specific heat of the target material are key parameters. Mean values of the specific heat between 0°C and the melting point and between the melting point and the boiling point were used in calculating the heat input as a function of the temperature reached for short bursts of energy input. The data used for 22 different metals ranging from magnesium to tungsten are shown in Table 5 with the results of the calculations presented in Table 5 and Figs. 9 and 10. The physical property data in the literature differ somewhat; the values in Table 5 were selected from Refs. 2, 7, 10, and 11.

An effort was made to make a similar set of calculations for some typical ceramic materials. The problem is complicated because many of the compounds of interest, for example,  $\text{Al}_2\text{O}_3$ ,  $\text{SiO}_2$ ,  $\text{SiC}$ , and  $\text{ZrO}_2$ , begin to decompose as they vaporize. Thus, not only may there be no

Table 5. Physical properties of some typical metals that might be used as armor or bumpers for spacecraft<sup>a</sup>

Metal	Atomic weight	Melting point (°C)	Boiling point (°C)	Heat of fusion (kcal/g mol)	Heat of vaporization (kcal/g mol)	$c_p$		Enthalpy above 0°C (J/g)				Sound velocity (m/s)
						°C to mp	mp to bp	To melting point	To liquid	To boiling point	To gas	
Magnesium	24.3	650	1,090	2.14	31.5	6.80	8.02	762	1,131	1,739	7,166	5,910
Lithium	6.9	179	1,317	1.10	32.5	6.9	6.9	749	1,417	6,182	25,903	
Beryllium	9.01	1,278	2,970	2.34	68.0	4.05	7.01	2,405	3,493	9,005	40,605	12,890
Aluminum	27.0	660	2,467	2.55	61.0	6.74	7.00	690	1,085	2,602	12,065	6,890
Titanium	47.9	1,675	3,260	4.50	102.5	7.3	8.9	1,069	1,462	2,695	11,655	6,560
Chromium	52.0	1,890	2,482	3.50	73.0	8.8	11.6	1,339	1,621	2,174	8,052	
Cadmium	112.4	321	765	1.48	32.2	7.1	7.1	85	140	257	1,457	
Iron	55.8	1,535	3,000	3.30	84.6	7.7	11.1	887	1,135	2,355	8,703	6,400
Cobalt	58.9	1,492	2,900	3.70	93.0	10.1	9.7	1,071	1,334	2,305	8,916	6,220
Nickel	58.7	1,453	2,732	4.21	89.6	7.47	10.1	774	1,074	1,996	8,387	5,910
Copper	63.5	1,083	2,595	3.12	72.8	6.15	7.5	440	641	1,393	6,194	5,250
Zinc	65.4	420	906	1.60	27.4	7.81	7.01	210	312	531	2,285	
Niobium	93	2,468	4,927	6.40	166.5	7.1	7.7	789	1,077	1,929	9,426	2,580
Molybdenum	96	2,610	5,560	6.60	142.0	9.1	8.5	1,036	1,324	2,417	8,611	6,250
Silver	108	961	2,212	2.65	61.6	6.5	7.4	242	345	704	3,092	3,940
Tungsten	184	3,410	5,927	8.42	197.0	7.1	7.4	551	743	1,166	5,649	5,750
Tin	118.7	232	2,270	1.72	68.0	6.9	9.0	56	117	764	3,163	
Rhenium	186	3,180	5,627	8.00	178.0	7.8	8.2	558	738	1,190	5,197	
Platinum	195	1,769	3,827	4.70	112.1	6.96	8.4	264	365	736	3,143	2,950
Gold	197	1,063	2,966	3.05	82.0	6.28	7.1	142	207	494	2,237	2,950
Bismuth	209	271	1,477	2.51	42.6	7.1	8.7	39	89	299	1,152	1,800
Lead	207	327	1,737	1.22	42.4	8.1	7.7	54	78	298	1,155	1,250

<sup>a</sup>Data selected from R. E. Bolz and G. L. Tuve, eds., *Handbook of Tables for Applied Engineering Science*, 2nd ed., CRC Press, Cleveland, 1973; G. P. Harnwell, *Principles of Electricity and Electromagnetism*, McGraw-Hill Book Co., Inc., New York, 1949; J. W. Victoreen, "The Calculation of X-ray Mass Absorption Coefficients in Practice," *J. Appl. Phys.* 20, 1141-47 (December 1949); *Handbook of Chemistry and Physics*, 40th ed., CRC Press, Cleveland, 1959; and *1980 Calendar and Reference Book*, Westinghouse Fusion Power Systems, Pittsburgh, 1980.

ORNL-DWG 85-4868 ETD

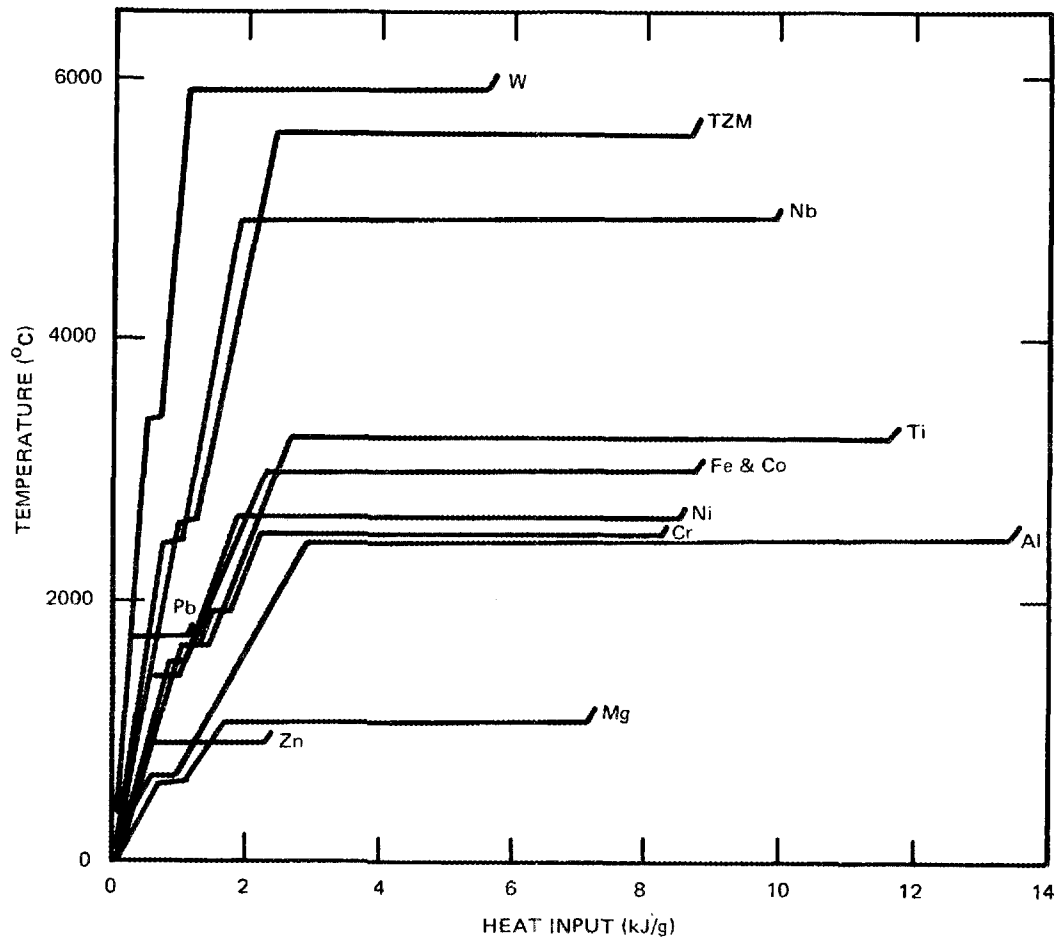


Fig. 9. Temperature rise from 0°C as a function of heat input for typical metals (data from Table 5).

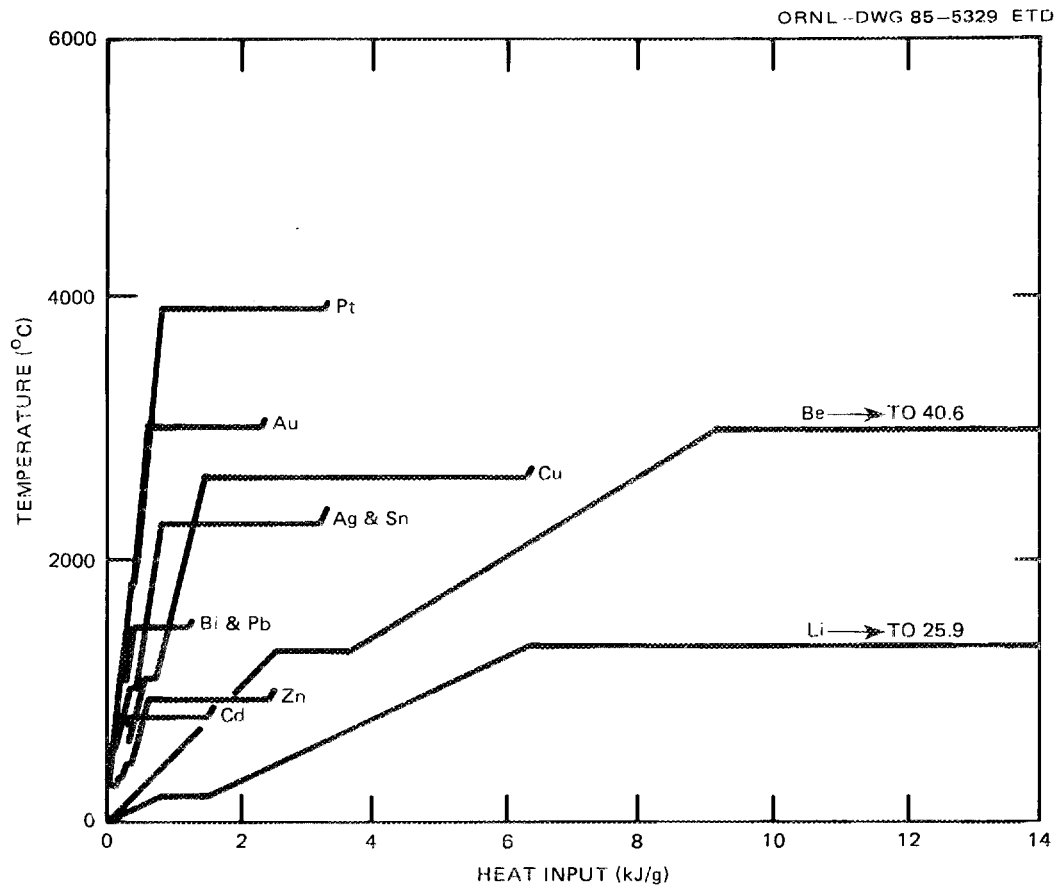


Fig. 10. Temperature rise above 0°C as a function of heat input for typical metals (data from Table 5).

true boiling point, but also the energy absorbed as a function of temperature in the region where the compounds vaporize probably varies with the heating rate for the short energy pulses of prime interest here. In an effort to gain some insight into the problem, experimental data for laser machining of ceramics were examined, but these data are difficult to interpret because much of the material ejected from the laser-heated region at the bottom of a hole being drilled comes off as tiny liquid droplets suspended in the vapor (see Refs. 4 and 5). This effect is evident in Table 6, calculated from data in Ref. 4. In this case, the heat input per gram of material removed from laser-drilled holes was only 30 to 50% of the heat required for complete vaporization. In considering possible damage to spacecraft, liquid droplets probably would not be entrained and carried away by the vapor, but, rather, the entire surface in the beam would be heated fairly uniformly. Therefore, the data for laser machining were not used, but values were calculated from basic thermodynamic data in Refs. 12-15.\* The resulting values given in Table 7 and Fig. 11 for the heat required to vaporize ceramics are, except for those for carbon, probably low because additional heat would be required for dissociation. Thus, they should be regarded as rough estimates, and better values should be obtained from experiments with laser beams.

Figures 9-11 are helpful in visualizing the effects of material choice on the severity of the damage to be expected. For example, almost twice as much heat per gram of material is required to melt magnesium as that required to melt tungsten; therefore, less energy in the form of a short pulse is required to melt a thin tungsten wall than a magnesium wall with the same mass. Also note that while the latent heats of fusion are relatively small, the heats of vaporization are greater than the amount of heat required to raise the temperature all the way from 0°C to the boiling point.

---

\*The writer is greatly indebted to T. Lindemer, R. Strehlow, and R. P. Wichner of Oak Ridge National Laboratory for their kind assistance in this work.

Table 6. Data from laser hole-drilling experiments

Material	Hole diameter (mm)	Depth (mm)	Energy (J)	Power (kW/cm <sup>2</sup> )	Time (s)	Enthalpy (J/g)
<i>Multipulse beam</i>						
Iron	0.05	1	0.05	60,000	90	3,181
	0.2	1	0.3	12,000	100	1,193
	0.1	0.7	1.5	20,000	1,000	34,079
Stainless steel	0.05	1.2	0.2	120,000	90	10,602
Brass	0.03	0.1	0.05	40,000	100	88,352
Ruby	0.01	0.4	0.1			397,583 <sup>a</sup>
Glass	0.05	0.6	0.3	50,000	100	31,807
Ceramic	0.2	3.2	1.4	4,000	500	1,739
<i>Single pulse beam</i>						
Iron	0.42	1.2	5.4		250	4,057
	0.39	1.3	5.1		350	4,102
	0.38	1.5	5.9		550	4,332
	0.36	1.6	5.7		750	4,372
	0.3	1.8	5.4		850	5,301
	0.26	1.6	5		1,150	7,352

<sup>a</sup>This high value probably resulted from use of a ruby laser beam.

Source: N. Rykalin et al., *Laser Machining and Welding*, tr. O. Glebov, Pergamon Press, New York, 1978.

Table 7. Energy required to heat and melt or heat and vaporize typical ceramics

Material	Molecular weight	Melting point (°C)	Boiling point <sup>a</sup> (°C)	Heat of fusion (kcal/g mol)	Heat of vaporization <sup>b</sup> (kcal/g mol)	Enthalpy above 0°C (J/g)			
						To melting point	To liquid	To boiling point	To gas
Al <sub>2</sub> O <sub>3</sub>	102	2,051	4,000	25.7	340	2,500	3,555	5,936	19,892
BeO	25	2,580	4,260	19.3	173	5,426	8,659	12,176	41,150
MgO	40.3	2,825	3,260	18.5	156	3,688	5,610	6,078	22,286
SiO <sub>2</sub>	60.1	1,722	3,460	2.6	137	2,020	2,201	4,222	13,766
ZrO <sub>2</sub>	123.2	2,680	4,100	20.8	167	1,679	2,386	3,283	8,959
Graphite	12	sublimes	3,600		170	5,652	5,652	16.2	64,968

<sup>a</sup>An explicit value for the boiling point was found only for MgO and C. Values for the others were estimated.

<sup>b</sup>The heat of vaporization was taken as the difference in the enthalpies of the ideal gas and the liquid or the crystalline solid, where no value was given for the liquid. For alumina it was assumed that the bulk of the vapor would be in the form of Al<sub>2</sub>O and O<sub>2</sub>.

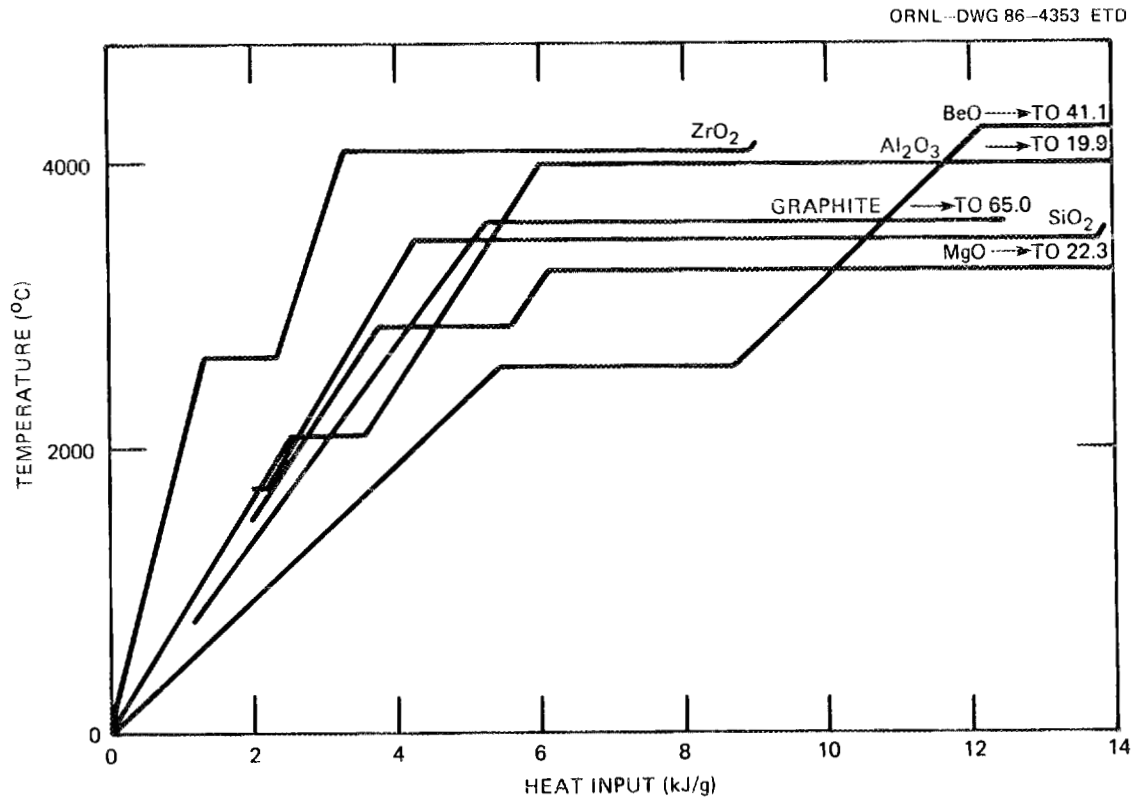


Fig. 11. Temperature rise as a function of heat input for typical ceramics (data from Table 7).

#### 4.2 Temperature Distribution in Short Bursts

When the duration of an energy pulse is short, the surface is heated much more rapidly than the subsurface material. Equations for the transient temperatures of plates that are exposed to short duration pulses of heat on one surface have been presented by Jakob.<sup>16</sup> Using Jakob's relations, Fig. 12 was prepared in the course of an earlier study on damage to the vacuum walls of thermonuclear reactors<sup>2</sup> to show the temperature distribution in an infinitely thick plate with uniform, temperature-independent properties following the sudden initiation of an energy input to the surface. (Computational methods are described in an appendix of Ref. 2.) The results are presented in terms of dimensionless parameters for the temperature, the distance from the heated surface, and the time from initiation of the energy pulse. Similar temperature distributions are presented in Fig. 13 for more-complex cases in which allowances were made for melting and vaporization. In Fig. 13 the abscissa is the distance from the heated face with allowance for the fact that it begins to recede after vaporization begins.

For any given pulse energy input and duration, the temperature distribution varies widely from one material to another as a consequence of differences in the thermal conductivity and heat capacity factors. To show these effects for a set of typical cases, a series of calculations was carried out for six different alloys, assuming no phase change. The results are summarized in Table 8 and shown graphically in Fig. 14. The effects of pulse time on the temperature distribution for a typical pulse energy are shown for aluminum in Fig. 15. The calculational procedure is presented in Appendix A.

It is evident from Fig. 14 and Table 8 that for a 50-J/cm<sup>2</sup> burst for 1-ms some of the titanium would be vaporized, and the stainless steel surface temperature would be close to the boiling point of chromium. Thus, it is interesting to calculate how short the pulse duration should be to bring the surface of the six alloys of Fig. 14 to the boiling point. This was done for several different pulse energies, and

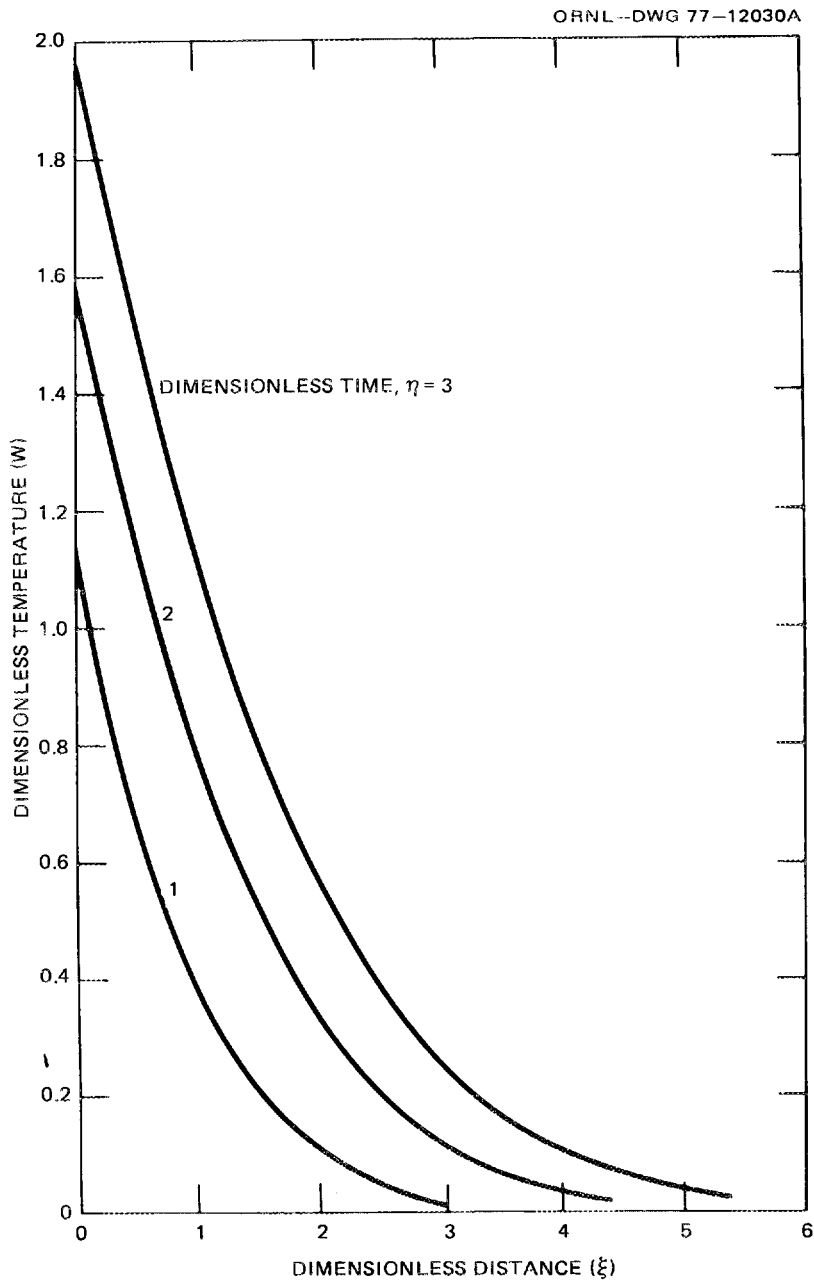


Fig. 12. Transient temperature distribution in a thick slab (latent heat of fusion neglected). *Source:* A. P. Fraas and A. S. Thompson, *ORNL Fusion Power Demonstration Study: Fluid Flow, Heat Transfer, and Stress Analysis Considerations in the Design of Blankets for Thermonuclear Reactors*, ORNL/TM-5960, Union Carbide Corp. Nuclear Div., Oak Ridge Natl. Lab., February 1978, p. 53.

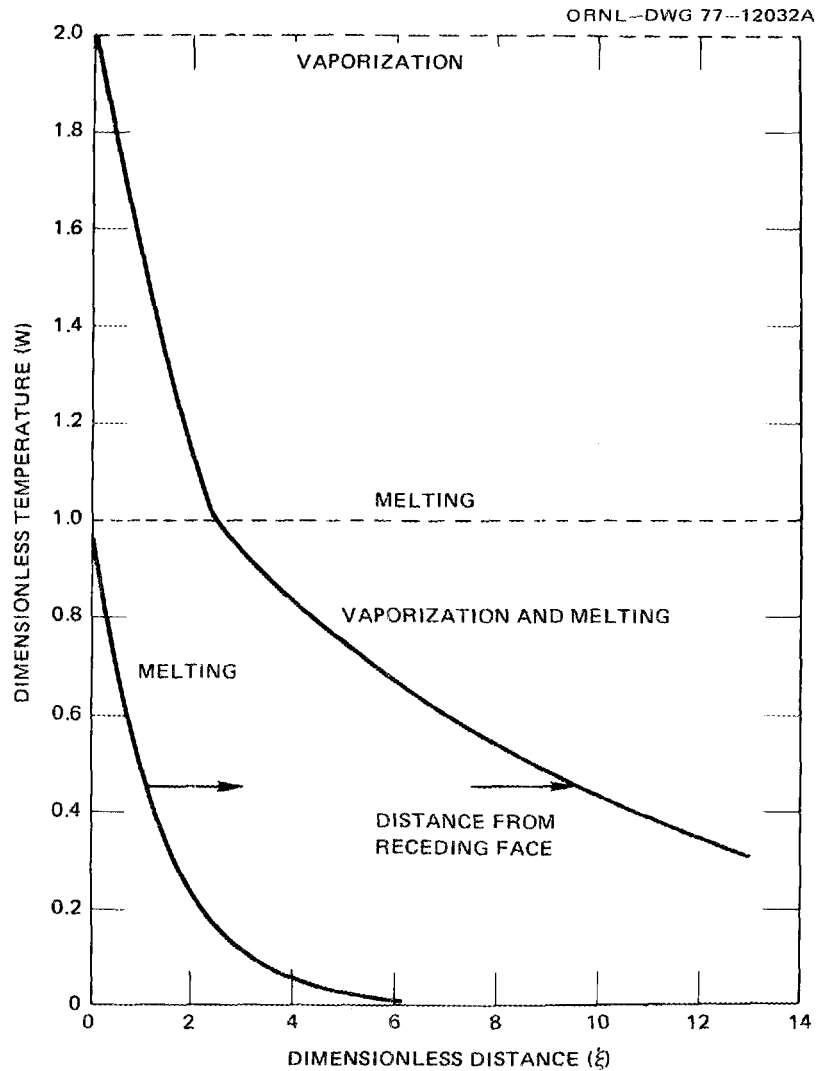


Fig. 13. Temperature distribution in a thick slab with steady state melting and vaporization. Source: A. P. Fraas and A. S. Thompson, *ORNL Fusion Power Demonstration Study: Fluid Flow, Heat Transfer, and Stress Analysis Considerations in the Design of Blankets for Thermonuclear Reactors*, ORNL/TM-5960, Union Carbide Corp. Nuclear Div., Oak Ridge Natl. Lab., February 1978, p. 55.

Table 8. Temperature distribution in thick slabs of various target materials,<sup>a</sup> initially at 0°C, following a surface heat pulse of 50 J/cm<sup>2</sup> in a period of 0.001 s<sup>b</sup>

u	g(u)	Mg		Al		Ti		SS		Nb		TZM	
		x <sup>c</sup>	T <sup>c</sup>	x	T	x	T	x	T	x	T	x	T
0	0.5642	0	980.6	0	741.4	0	3923.0	0	2153.0	0	1413.0	0	1048.0
0.1	0.4698	0.0054	816.4	0.0062	617.4	0.0013	3267.0	0.0012	1793.0	0.0035	1176.0	0.0039	872.7
0.2	0.3866	0.0108	671.8	0.0125	508.0	0.0027	2688.0	0.0024	1475.0	0.0069	967.9	0.0078	718.1
0.3	0.3142	0.0163	546.0	0.0187	412.9	0.0040	2185.0	0.0036	1199.0	0.0104	786.7	0.0117	583.7
0.4	0.2522	0.0217	438.3	0.0249	331.4	0.0054	1754.0	0.0049	962.3	0.0138	631.4	0.0156	468.5
0.5	0.1996	0.0271	346.9	0.0311	262.3	0.0067	1388.0	0.0061	761.6	0.0173	499.7	0.0195	370.8
0.6	0.1559	0.0325	270.9	0.0374	204.9	0.0081	1084.0	0.0073	594.8	0.0209	390.3	0.0234	289.6
0.7	0.1201	0.0380	208.7	0.0436	157.8	0.0094	835.1	0.0085	458.3	0.0242	300.7	0.0273	223.1
0.9	0.0682	0.0488	118.5	0.0561	89.6	0.0121	474.2	0.0109	260.2	0.0311	170.8	0.0351	126.7
1.0	0.0503	0.0542	87.4	0.0623	66.1	0.0135	349.8	0.0121	191.9	0.0346	125.9	0.0390	93.4
1.2	0.0261	0.0651	45.4	0.0747	34.3	0.0162	181.5	0.0146	99.6	0.0415	65.4	0.0468	48.5
1.5	0.0086	0.0813	14.9	0.0934	11.3	0.0202	59.8	0.0182	32.8	0.0518	21.5	0.0585	16.0
2.0	0.0009	0.1084	1.6	0.1246	1.2	0.0270	6.3	0.0243	3.4	0.0691	2.3	0.0780	1.7
3.0	0.0001	0.1627	0.2	0.1869	0.1	0.0405	0.7	0.0364	0.4	0.1037	0.3	0.1170	0.2

<sup>a</sup> Physical properties	Mg	Al	Ti	SS	Nb	TZM
k, W/cm °C	1.56	2.37	0.097	0.159	0.69	1.05
c <sub>p</sub> , J/g °C	1.22	0.905	0.52	0.54	0.272	0.276
ρ, g/cm <sup>3</sup>	1.74	2.7	4.1	8.0	8.5	10.0
γ = k/c <sub>p</sub> ρ	0.7349	0.9699	0.0455	0.0368	0.2984	0.3804
$\sqrt{\gamma\tau}$	0.0542	0.0623	0.0135	0.0121	0.0346	0.0390
Temperature rise coefficient (2Q/√kc <sub>p</sub> ρτ)	1738	1314	6954	3816	2504	1858

<sup>b</sup>See Appendix A for definition of symbols and method of calculation.

<sup>c</sup>x is in centimeters, and T is in degrees Celsius.

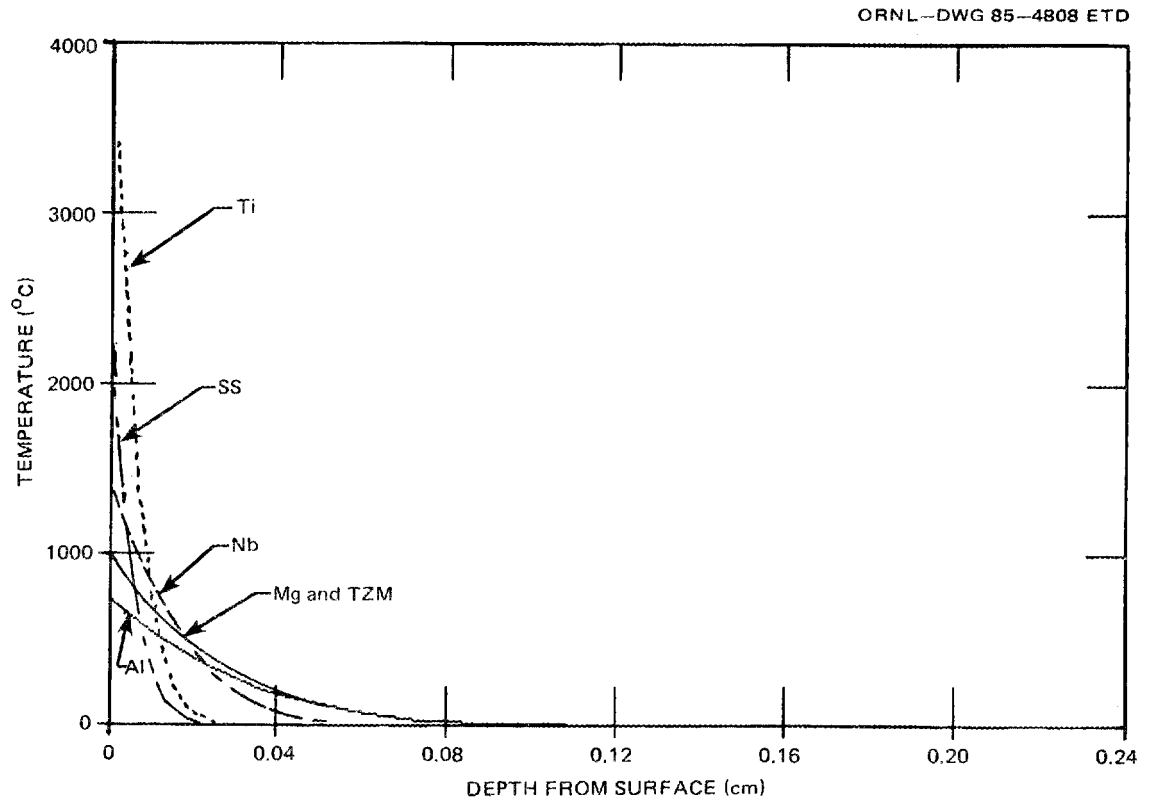


Fig. 14. Temperature distribution in typical alloys after a 1-ms pulse of  $50\text{-J/cm}^2$  energy input to the surface (data from Table 8).

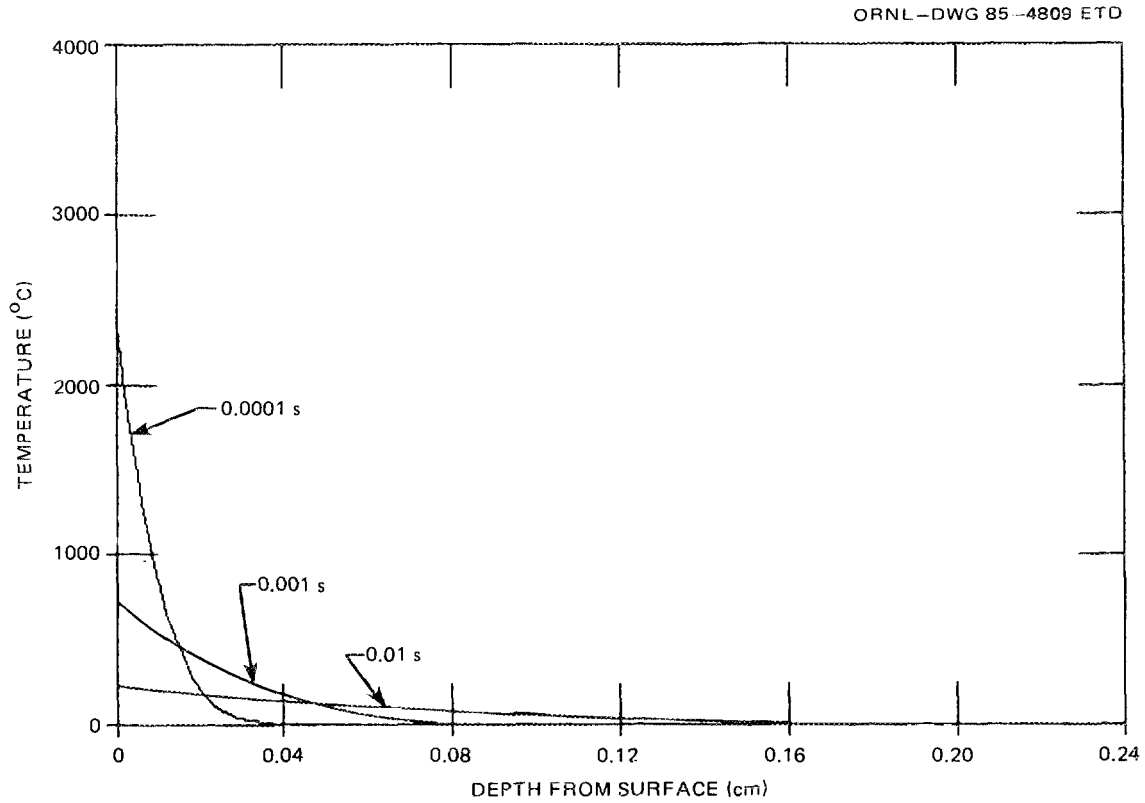


Fig. 15. Effects of 0.01-, 0.001-, and 0.0001-s pulse durations on the temperature distribution in aluminum after a  $50\text{-J/cm}^2$  energy input to the surface.

the results are presented in Table 9 and Fig. 16. The procedure for these calculations is included in Appendix A.

#### 4.3 Explosive Vaporization

Probably the most significant implications of the preceding temperature distributions are those associated with pulse durations of  $<0.1$  ms. Relatively little beam energy is required to raise the surface temperature to the boiling point for these short pulses; thus, any additional beam energy will be utilized to form vapor. This is important because abrupt vaporization of a substantial amount of material will produce an explosive blast effect. In fact, if the pulse time is  $\sim 0.1$   $\mu$ s, the vaporization takes place in a time shorter than that required for a pressure wave to move at the speed of sound through the metal; thus, a potentially extremely destructive detonation wave results. Further, for a pulse duration of only  $10^{-7}$  s, Fig. 16 shows that only  $0.5$  J/cm<sup>2</sup> is required to raise the surface temperature of stainless steel to the boiling point. To put the matter in more familiar terms, the energy release in the detonation of a gram of high explosive is  $\sim 4000$  J/g; thus, putting 50 J/g into metal vapor would give an explosive force roughly equivalent to detonating 10 mg/cm<sup>2</sup> of high explosive. An energy burst of 50 J/cm<sup>2</sup> will serve to heat and vaporize 0.006 g of iron. The effect would be comparable to detonating 0.01 g/cm<sup>2</sup> of high explosive plastered over the irradiated surface. This would amount to  $\sim 100$  g/m<sup>2</sup> of high explosive and would have roughly the same destructive effect as one stick of dynamite. (Actually, for a given energy release, the force of an explosion increases with the square root of the molecular weight of the vapor, and this would be higher for iron than for a high explosive.) Such an explosion would be quite destructive to the light structures of spacecraft. Thus, for a system in which the total energy input is an important factor, there is a strong incentive to employ beams with pulse durations of  $<0.01$  ms and, preferably,  $<10^{-7}$  s.

In attempting to appraise the possible blast damage from explosive vaporization, the first step was to estimate the instantaneous blast

Table 9. Pulse duration for incipient vaporization at the surface of six alloys

Parameter	Material					
	Mg	Al	Ti	SS	Nb	TZM
<i>Physical properties</i>						
Boiling point, $T_v$ , °C	1090	2467	3260	3000	4927	5560
$c_p^*$ , J/g, °C <sup>a</sup>	1.595	1.192	0.827	0.785	0.392	0.435
$\rho_p^*$ , g/cm <sup>3</sup>	1.74	2.7	4.1	8.0	8.5	10.0
$k$ , W/cm °C	1.3	1.7	0.17	0.16	0.37	0.91
$\tau = \text{Pulse duration (s)}^b$						
Pulse energy, $Q$ , J/cm <sup>2</sup>						
50	0.0010346	0.0001332	0.0007240	0.0004904	0.0001482	0.0000362
20	0.0001655	0.0000213	0.0001158	0.0000785	0.0000237	0.0000058
10	0.0000414	0.0000053	0.0000290	0.0000196	0.0000059	0.0000014

<sup>a</sup>  $c_p^* = (\text{enthalpy change from } 0^\circ\text{C to boiling point, J}) / (\text{boiling point, } ^\circ\text{C})$ .

$$^b \tau = \frac{1}{\pi k c_p^* \rho} \frac{2Q^2}{T_v}$$

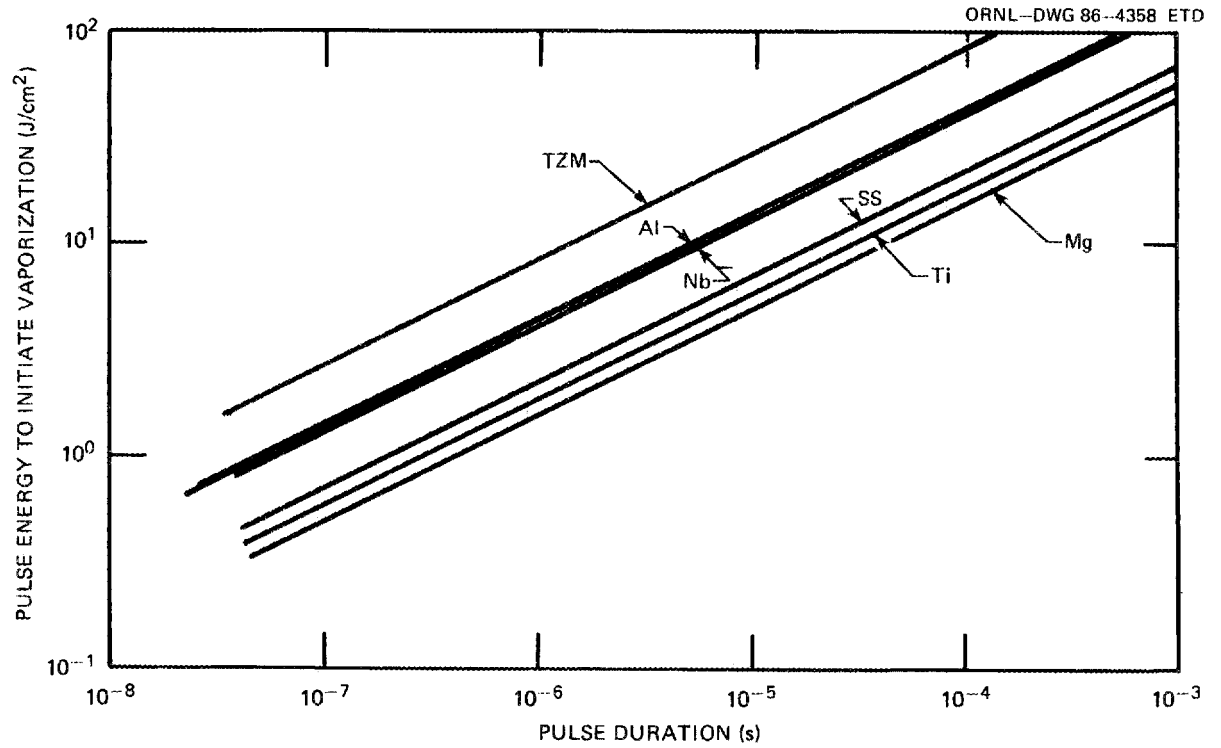


Fig. 16. Amount of energy in short pulses required to initiate vaporization in typical metals (data from Table 9).

pressure. A first rough approximation was calculated from the impulse imparted to the damaged surface by the momentum of the vaporized material,<sup>17</sup> assuming that it left the surface at the velocity of sound in the vapor at the boiling point of the metal. Table 10 summarizes the calculations, and Fig. 17 shows estimates of the blast pressure generated by the deposition of 10, 20, and 50 J/cm<sup>2</sup> to an aluminum surface. Figure 18 compares the effects of 50-J/cm<sup>2</sup> bursts on magnesium, titanium, and steel surfaces. The calculational procedure is summarized in Appendix B.

Table 10 and Figs. 17 and 18 are based on the amount of energy deposited in the surface (i.e., the energy in the incident beam minus the energy reflected). However, specular and diffuse radiations are not the only mechanisms reducing the beam energy input to the target; for the relatively high rates of energy input of interest here, the material vaporized from the surface may be ionized, and the ionized vapor itself absorbs light from the beam. Both analyses and experiments (see Refs. 18--21) show that these effects can be so large that the ionized vapor from the initial portion of the burst may be surprisingly effective in protecting the surface from further damage.

The ratio of the energy absorbed in the surface to the energy in the incident beam is called the "coupling coefficient." Some typical values determined for this parameter, as obtained by Nichols and Hall,<sup>19</sup> are shown in Fig. 19 for cases in which 2.8  $\mu$ m radiation from a hydrogen fluoride laser was directed at an aluminum target in pulses of from 3 to 4  $\mu$ s. The diameter of the beam at which the intensity was one-half the maximum was  $\sim$ 0.47 cm. Figure 19 shows that for low beam energies,  $\sim$ 94% of the incident energy in the beam is reflected (as one would expect). When the beam energy intensity exceeds  $\sim$ 100 J/cm<sup>2</sup>, a surface plasma is ignited that enhances thermal coupling to the target. Still further increases in beam energy intensity beyond  $\sim$ 200 J/cm<sup>2</sup> induce a laser-supported detonation (LSD) wave in the plasma. This moves rapidly away from the target and, by absorbing energy from the beam, reduces the fraction of the beam energy reaching the target. Thus, the fraction of the beam energy deposited in the target surface per pulse falls off

Table 10. Blast pressures from aluminum surface vaporization

	Pulse time (s)			
	10 <sup>-7</sup>	10 <sup>-6</sup>	10 <sup>-5</sup>	10 <sup>-4</sup>
	Vapor temperature -- 2740 K			
Atomic weight -- 27				
Vapor velocity -- 11 km/s				
Heat to vaporize -- 13,471 J/g				
Energy to preheat, J/cm <sup>2</sup>	1.93	6.1	19.3	61
<u>Pulse energy = 50 J/cm<sup>2</sup></u>				
Mass vaporized, g/cm <sup>2</sup>	0.0036	0.0033	0.0023	0
Blast pressure, bar	3975	363	25	0
<u>Pulse energy = 20 J/cm<sup>2</sup></u>				
Mass vaporized, g/cm <sup>2</sup>	0.0013	0.0010	0.0001	0
Blast pressure, bar	1494	115	<1	0
<u>Pulse energy = 10 J/cm<sup>2</sup></u>				
Mass vaporized, g/cm <sup>2</sup>	0.0006	0.0003	0	0
Blast pressure, bar	667	32	0	0

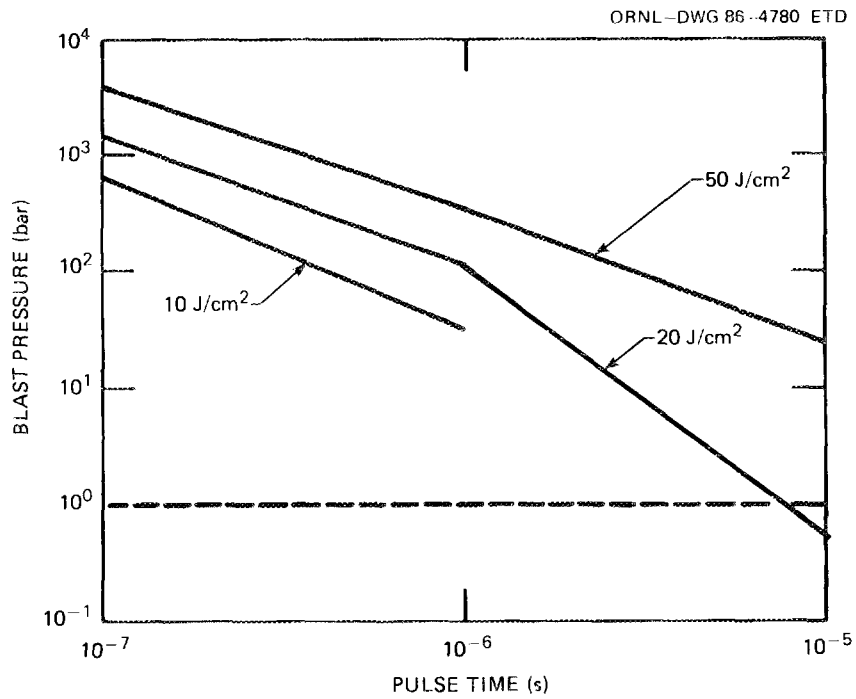


Fig. 17. Blast pressures generated by short burst of energy input to an aluminum surface (data from Table 10).

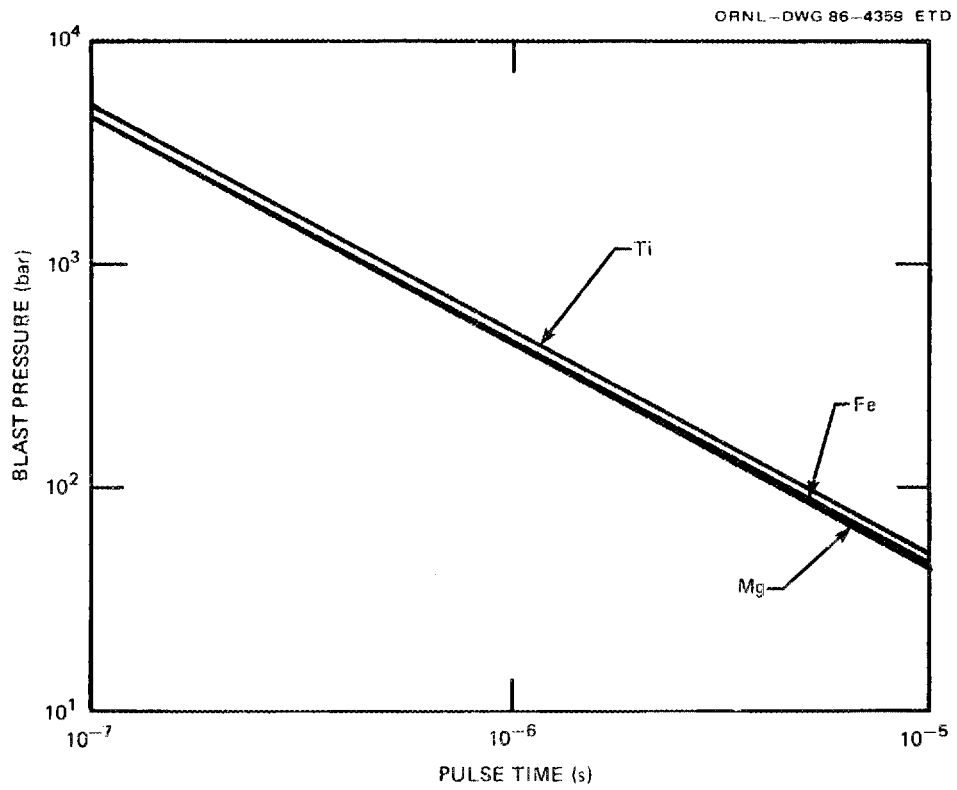


Fig. 18. Blast pressures generated by  $50\text{-J/cm}^2$  energy inputs to magnesium, titanium, and steel surfaces.

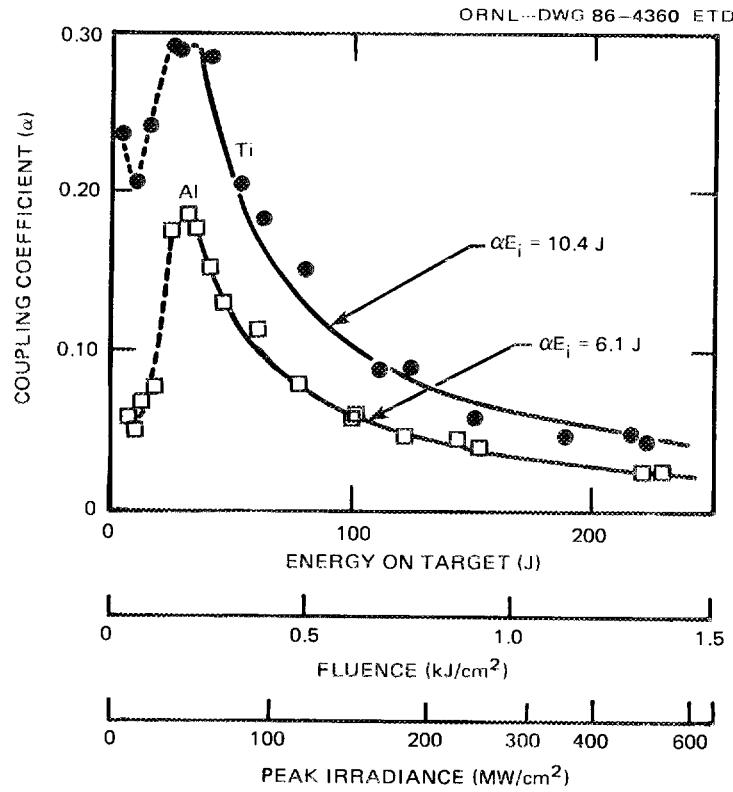


Fig. 19. Coupling coefficient as a function of beam energy intensity for pulse durations of 3 to 4  $\mu\text{s}$  from a 2.8- $\mu\text{m}$  HF laser. *Source:* D. B. Nichols and R. B. Hall, "Thermal Coupling of 2.8  $\mu\text{m}$  Laser Radiation to Metal Targets," *AIAA J.* 18(4), 476-78 (April 1980), p. 477.

rapidly with further increases in pulse energy; the total amount of energy deposited in the target, however, increases at a progressively lower rate. Note that an arrow in Fig. 19 marks the point at which the product of the coupling coefficient and the energy in the incident beam gave 10.4 J ( $\sim 66 \text{ J/cm}^2$ ) deposited in the titanium surface; a similar arrow marks the point where 6.1 J were deposited in the aluminum surface. Similar tests run with nickel and stainless steel yielded roughly similar results, with the coupling coefficient for stainless steel a little higher than that for titanium and the coefficient for nickel a little higher than that for aluminum. Note that the tests of Fig. 19 were run in air so that ionization of the air occurred, but the authors also reported other tests with aluminum and titanium in which the data for both air and vacuum conditions fell within the same scatterband. This is not surprising because the atomic weight of aluminum is 27, that of titanium is 48, and the molecular weight of air is 28.97.

The blast pressure induced in the target by the LSD wave was measured in an interesting series of tests.<sup>20</sup> Figure 20 shows the peak pressure at the target surface as a function of the peak intensity of a 1.06- $\mu\text{m}$  beam from a neodymium glass laser with a maximum output of 125 J, irrespective of pulse time. About 75% of the beam energy fell within a 0.25-cm-diam circle. Note that increasing the peak beam intensity beyond  $\sim 3 \times 10^8 \text{ W/cm}^2$  (a 1- $\mu\text{s}$  pulse of  $\sim 300 \text{ J/cm}^2$ ) actually led to a decrease in the pressure of the detonation wave.

From the standpoint of damage to spacecraft structures, the impulse imparted to the target is a more important parameter than the instantaneous blast pressure. Thus, the tests of Ref. 20 included measurements of this impulse; typical data are presented in Fig. 21 in terms of the impulse in dyne-seconds per joule of energy input. Note that the maximum impulse per unit of beam energy was obtained with a beam energy  $\sim 25\%$  of that for the maximum blast pressure indicated by Fig. 20.

Although the blast pressures of Figs. 17, 18, and 20 are extremely high, they are of such short duration that their effects are limited by the inertia of the surface, as well as by its strength and elastic characteristics. The controlling parameter — the impulse, or momentum,

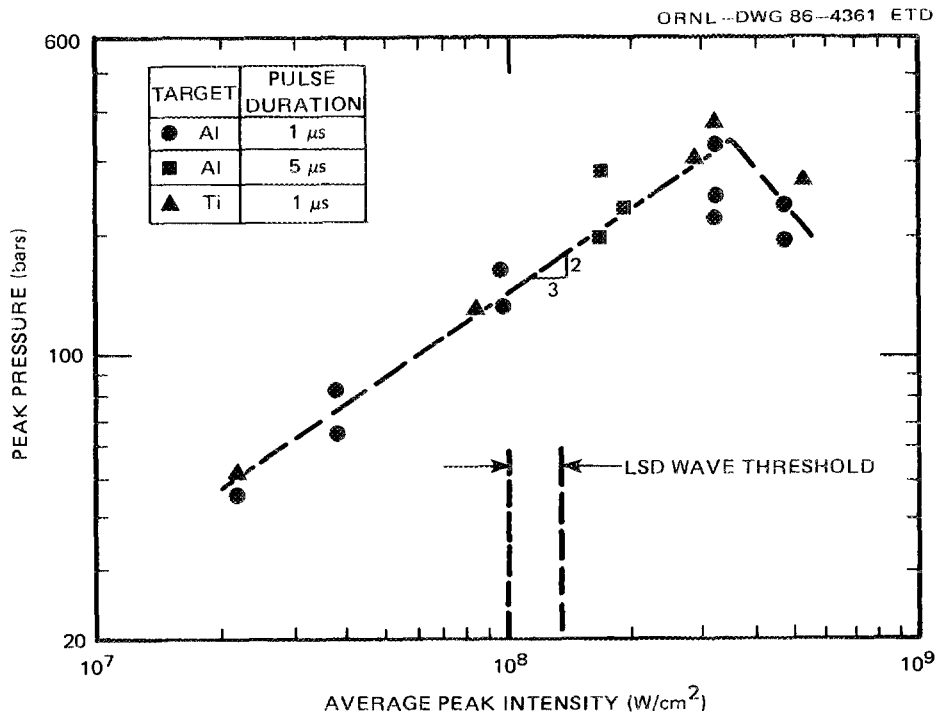


Fig. 20. Peak pressure induced in aluminum and titanium targets by laser-supported detonation (LSD) waves, plotted as a function of peak intensity of a beam from a 1.06- $\mu$ m neodymium glass laser. *Source:* L. R. Hettele et al., "Mechanical Response and Thermal Coupling of Metallic Targets to High-Intensity 1.06  $\mu$ m Laser Radiation," *J. Appl. Phys.* 47(4), 1415-21 (April 1976), p. 1419.

ORNL-DWG 86-4766 ETD

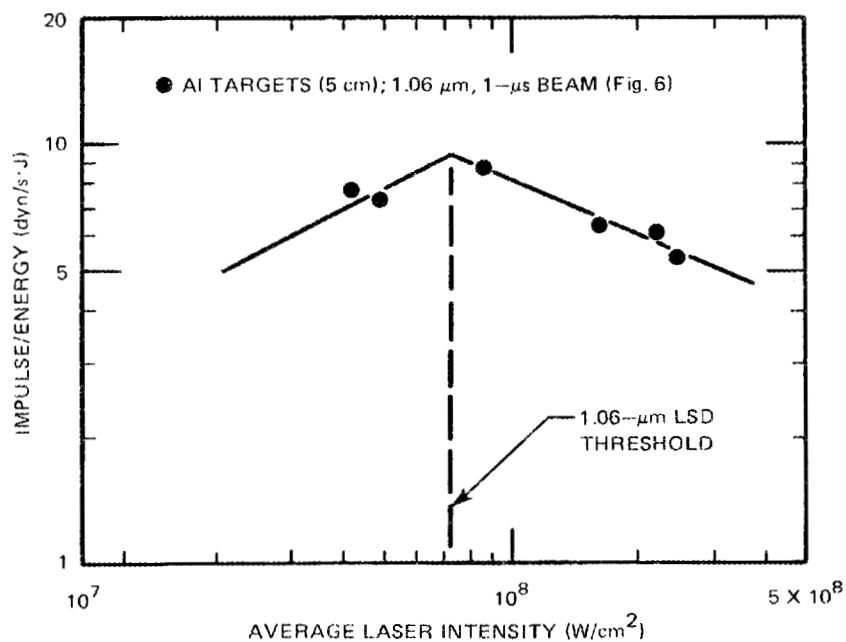


Fig. 21. Impulse imparted to an aluminum target per joule of energy in the incident beam as a function of the energy in a 1.06- $\mu\text{m}$  beam with pulse duration of 1  $\mu\text{s}$ . Note discontinuity at threshold for laser-supported detonation (LSD). Source: L. R. Hettele et al., "Mechanical Response and Thermal Coupling of Metallic Targets to High-Intensity 1.06  $\mu\text{m}$  Laser Radiation," *J. Appl. Phys.* 47(4), 1415-21 (April 1976), p. 1418.

imparted to the structure — equals the product of the mass vaporized and the vapor velocity leaving the surface. The deflection of the structure required to absorb this impulse will depend on the ratio of the pulse time to the period for the natural frequency of vibration of the structure for the induced deflection mode.

It is evident from this brief discussion that whether the blast causes damage depends on the particular structure. The key parameters are the momentum (or impulse) imparted to the surface, the inertia of the structure, its strength, and the character of its elastic deformation under load, that is, its ability to absorb the impulse load elastically without excessive stresses in regions of stress concentrations. A thin-walled vessel might deform elastically from a circular to an oval cross section from which it might snap back without buckling. Although filling the vessel with liquid would increase the effective inertia of its wall, it would also increase its rigidity, and the pressure pulse in the confined liquid might lead to rupture at a stress concentration in a riveted seam in hoop tension. If made of a brittle material, the structure would be subject to the shattering effects of shock waves generated by pulses of  $<10^{-7}$  s. These effects can be examined by elegant and somewhat tricky calculations for any particular structure, but it is not possible to give any easily applicable generalizations. In any case, it would be wise to confirm analyses by tests with explosives using properly scaled mock-ups of the structures and an appropriate explosive.

#### 4.4 Thermal Stresses

It has been suggested that a rapidly pulsed beam of moderate energy density might be employed to induce damaging thermal stresses. A relatively thin, brittle structure might be shattered by the thermal stresses induced in a single pulse, but in a more massive structure (such as a nose cone for reentry) a single pulse would probably just cause spalling of flakes from the surface. Pulse repetition at a slow rate could cause serious erosion, but it is unlikely that the beam could

be held directly on the target for long enough to make this approach effective.

In ductile metals severe thermal stresses are alleviated by plastic flow so that cracking rarely occurs in a single cycle. Repeated surface heating pulses producing transient temperature distributions obviously induce biaxial tensile stresses in the surface. These can cause a type of failure (known as "thermal strain cycling") in a material as tough as Inconel. In a typical example the failure took the form of a network of surface cracks, as shown in Fig. 22 (from Ref. 22). The number of cycles to produce failure depends on the severity of the thermal strain, that is, (1) the temperature range through which the surface temperature fluctuates per cycle and (2) the properties of the metal.<sup>23</sup> Figure 23 is included here to facilitate the appraisal of possible damage from thermal stresses, although it appears that 10 to 100 cycles would be required to cause serious damage. This failure mode, therefore, is not likely to be of much interest.

#### 4.5 Overall View of Failure Modes

A good perspective on the effects of pulse time on the character of the damage from energy pulse inputs to surfaces is given in Fig. 24; Fig. 25 shows the energy density and pulse time for some actual cases. (These charts are from Ref. 2, which gives further details.) Serious study of these charts, particularly Fig. 24, should serve to tie the previous discussion together and should prove more instructive than further discussion.

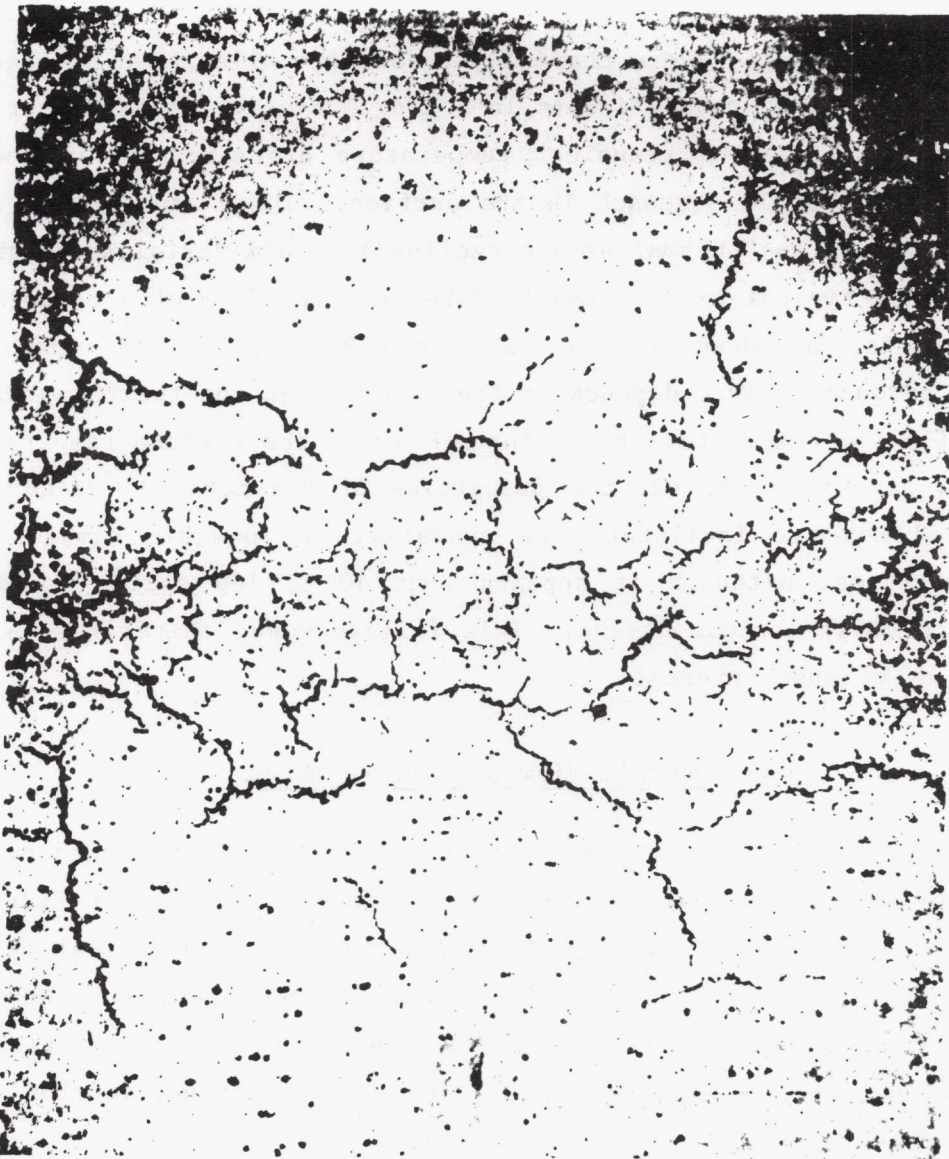


Fig. 22. Photo of interior surface of Inconel tube subjected to thermal-strain cycling at  $600^{\circ}\text{C}$  by temperature variation of  $60^{\circ}\text{C}$  in stream of molten salt. Number of cycles to failure was  $\sim 10^5$ . Source: J. J. Keyes and A. I. Krakoviak, "High Frequency Surface Thermal Fatigue Cycling of Inconel at  $1406^{\circ}\text{F}$ ," *Nucl. Sci. Eng.* 9(4), 462-66 (April 1961), p. 463.

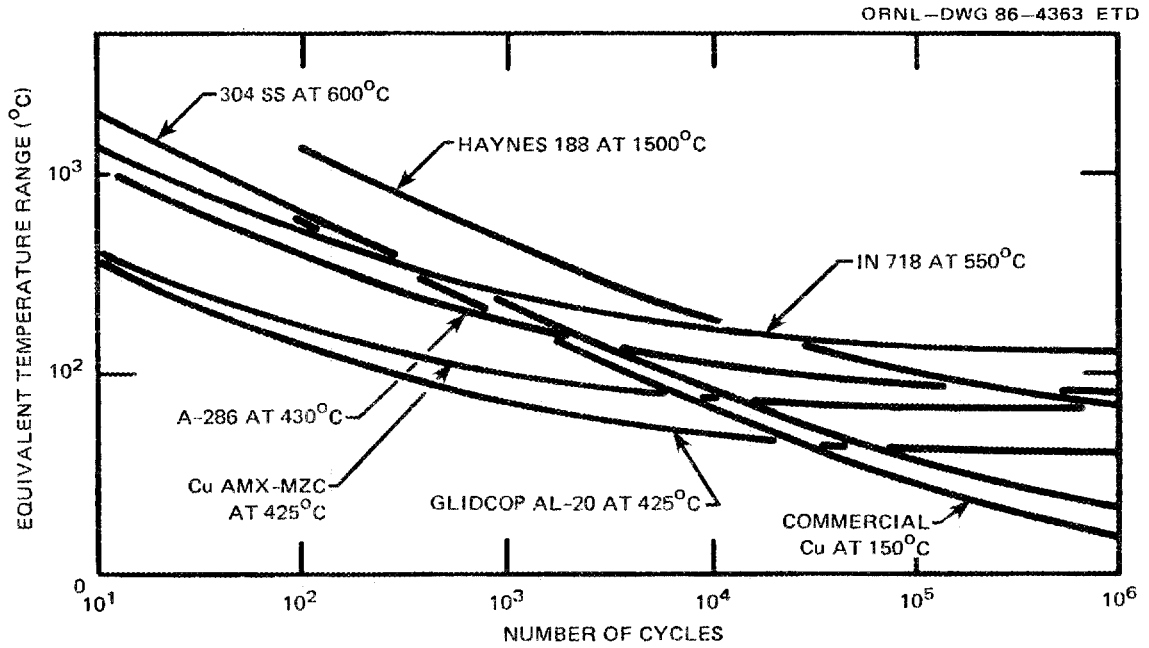


Fig. 23. Equivalent temperature range as a function of number of cycles to failure as calculated for typical alloys. Source: A. P. Fraas, *Engineering Evaluation of Energy Systems*, McGraw-Hill Book Co., Inc., New York, 1982, p. 163.

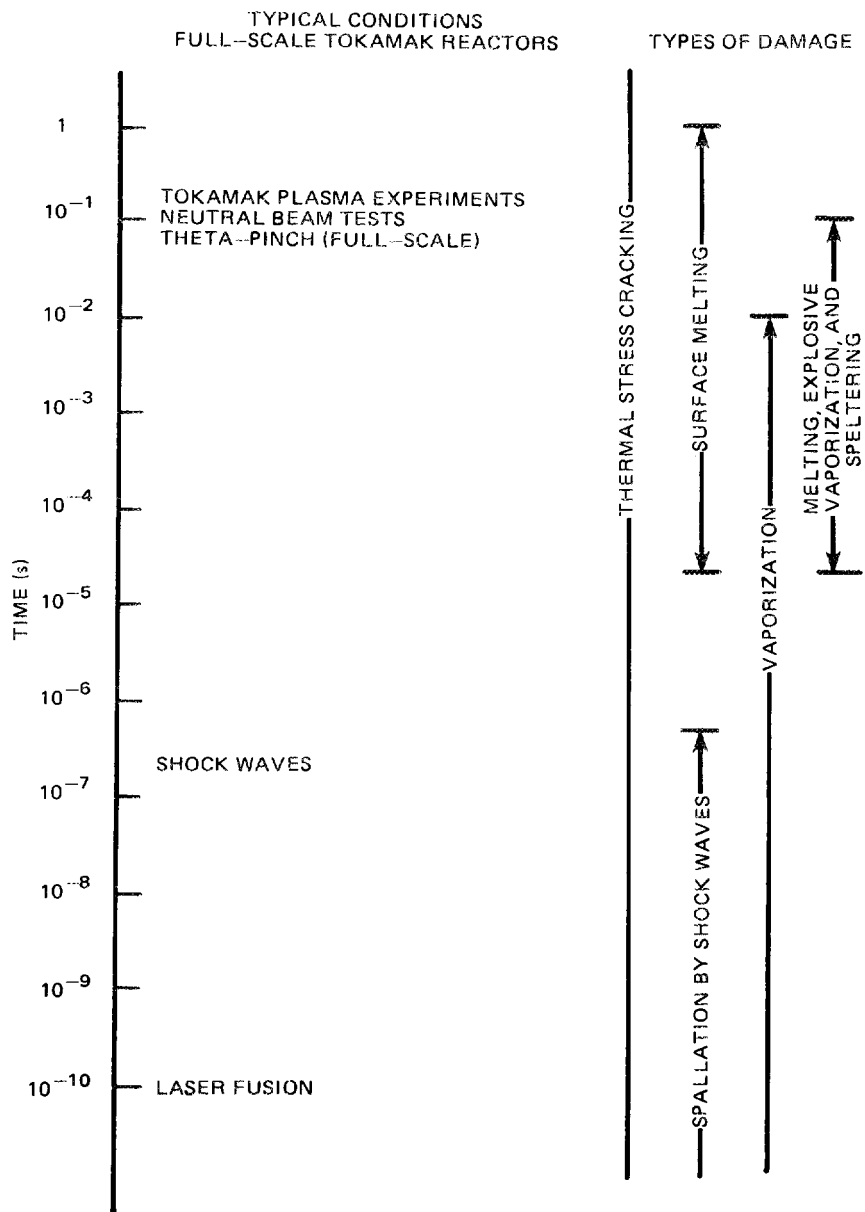


Fig. 24. Relation between types of surface damage and pulse times for typical cases. Source: A. P. Fraas and A. S. Thompson, *ORNL Fusion Power Demonstration Study: Fluid Flow, Heat Transfer, and Stress Analysis Considerations in the Design of Blankets for Thermonuclear Reactors*, ORNL/TM-5960, Union Carbide Corp. Nuclear Div., Oak Ridge Natl. Lab., February 1978, p. 48.

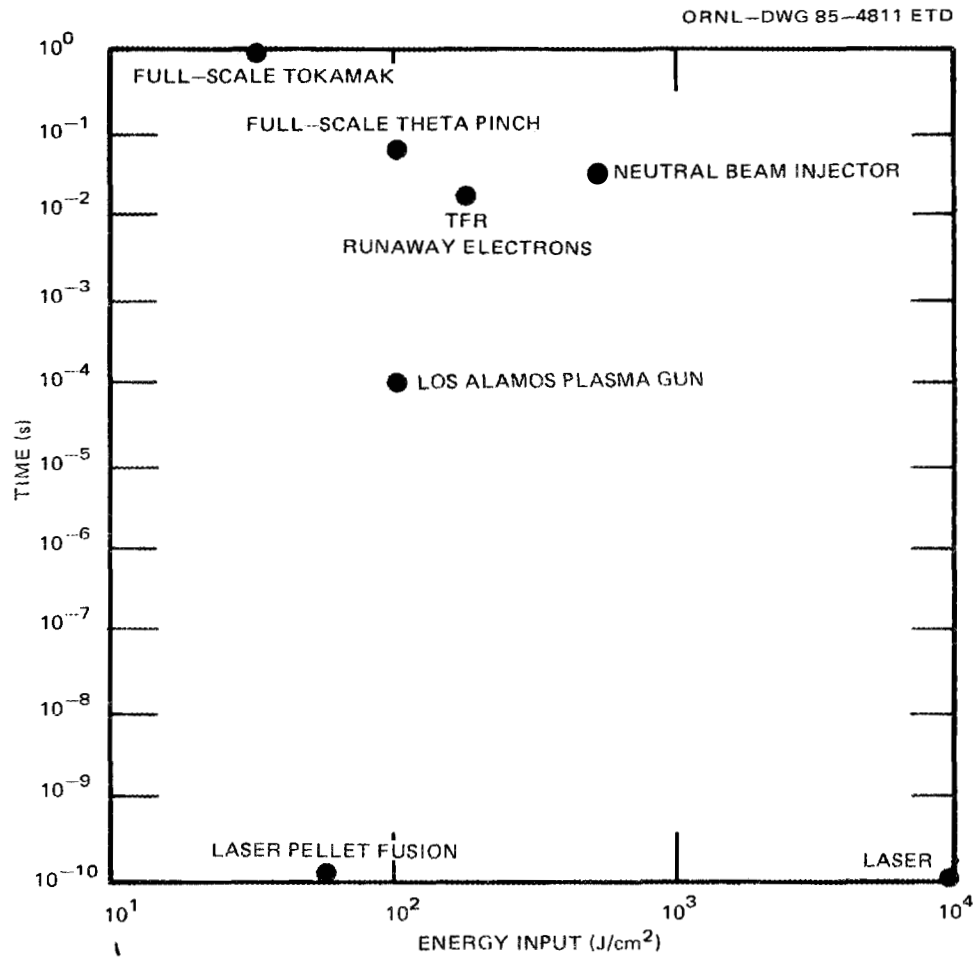


Fig. 25. Energy input per pulse for typical cases. *Source:* A. P. Fraas and A. S. Thompson, *ORNL Fusion Power Demonstration Study: Fluid Flow, Heat Transfer, and Stress Analysis Considerations in the Design of Blankets for Thermonuclear Reactors*, ORNL/TM-5960, Union Carbide Corp. Nuclear Div., Oak Ridge Natl. Lab., February 1978, p. 50.



## 5. SURVEY OF SOME TYPICAL CASES

### 5.1 Relations Between Pulse Energy, Duration, and Power

Figure 26 shows the relations between the energy input per pulse, the pulse time (or duration), and the rate of energy input (or power) during the pulse. The diagonal lines for a series of constant power input rates also indicate the equilibrium black-body temperature for that rate of energy dissipation. The scales at the right indicate the average temperature rise in 1-mm-thick plates of two typical materials, iron and aluminum, that would be produced by a burst of energy defined by the scale at the left. This chart is useful for appraising a wide variety of cases, but it must be remembered that it is for the actual energy input to the surface. Thus, when estimating the temperature rise in a surface heated by a laser beam, allowance must be made for the fact that a portion of the light in the beam will be reflected from the surface. For a radiator surface treated to give it a high emissivity, say 0.90, just 10% will be reflected, and 90% of the beam energy will be absorbed. To a first approximation the surface emittance will be the same as the absorptivity, and if the beam is continuous, the equilibrium temperature will be the same as would be the case for a black body for which 100% of the beam energy would be absorbed and then re-emitted with an emittance of 1.0. For bursts of energy input, however, the situation is quite different, especially if the reflectivity of the surface is fairly high. Consider, for example, a polished aluminum surface with a reflectivity of 0.85 for which only 15% of the incident light energy would be absorbed. The consequent temperature rise caused by the burst would be only 15% as great as for a black body. Of course, the rate of heat dissipation following the burst would also be only 15% as great, so the time for the temperature to return to equilibrium from a given energy pulse input would be the same as for a black body. The time to return to equilibrium from a given temperature excursion would be about six times as great.

In using Fig. 26 it must be remembered that both the reflectivity and the emittance of the surface must be considered. This is particularly important for special coatings whose emittance at the emitting

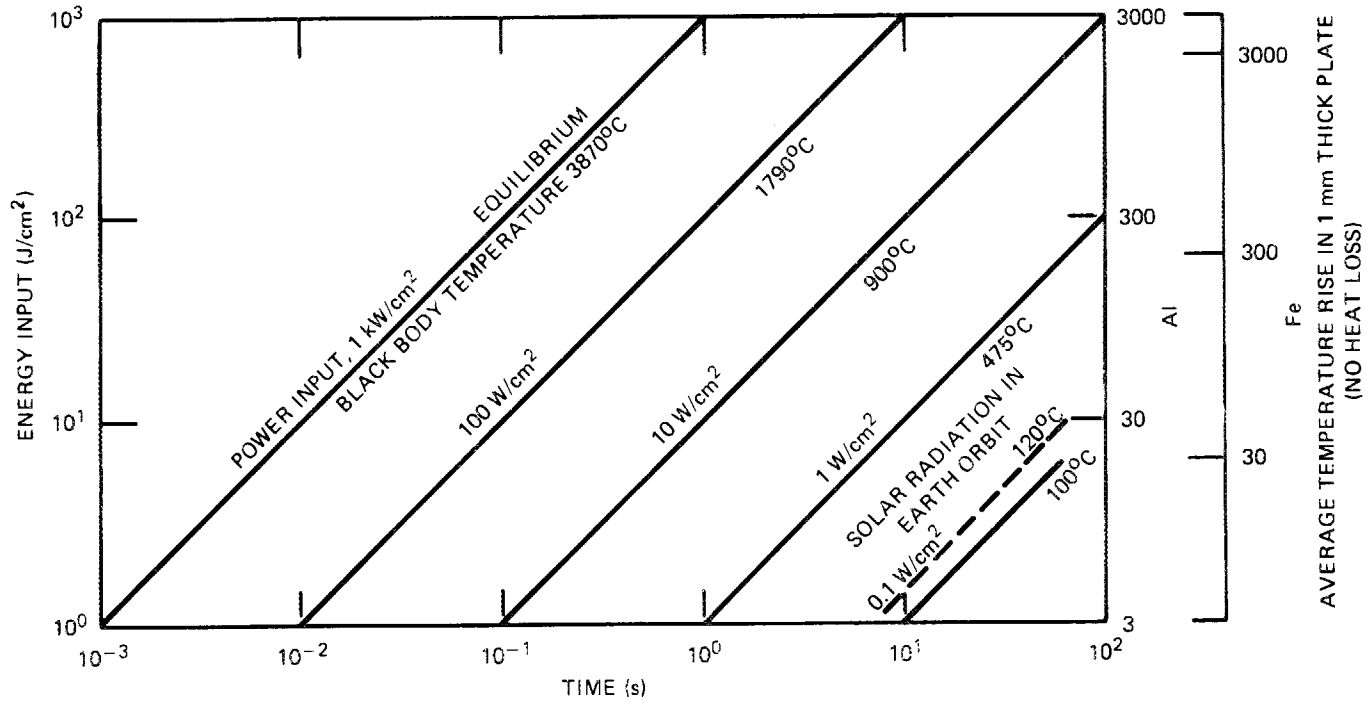


Fig. 26. Energy input vs time for series of beam power inputs.

temperature may be quite different from the absorptivity at the wavelength of the incident radiation. For example, aluminum oxide has a high total reflectivity in the visible light range, yet its emissivity in the infrared is also high (see Fig. 27, taken from Ref. 24). Similarly, although the writer has been unable to locate a reference that he saw in the latter 1960s, it is his recollection that a plasma-sprayed coating of zirconia (which is white) has both a high diffuse reflectivity for solar spectrum radiation and a high emissivity for infrared radiation at  $\sim 800$  K, probably in part because of cavity effects.

One highly pertinent case to consider is that of a solar cell array in which the semiconductor material or the soldered connections would be permanently damaged if the temperature were to reach  $375^\circ\text{C}$ . The light absorptivity is inherently high for efficient solar cells. It can be seen from Fig. 26 that a continuous energy input of  $1\text{ W/cm}^2$  would heat the cells to an equilibrium temperature of  $375^\circ\text{C}$ , thus putting them out of action. It can also be deduced from Fig. 26 that if the heat capacity of the cells per square centimeter were one-half that of a 1-mm thickness of iron, a short burst of  $\sim 50\text{ J/cm}^2$  would accomplish the same purpose with a smaller total energy input. On the other hand, if a space power plant having a niobium radiator with a tube wall thickness of 2 mm were subjected to the same intensities of radiation, the radiator would have its temperature increased by  $\sim 30^\circ\text{C}$  from the normal operating value of  $800^\circ\text{C}$  if exposed to a  $1\text{-W/cm}^2$  continuous beam, or the temperature would rise briefly by  $\sim 100^\circ\text{C}$  if exposed to a  $50\text{-J/cm}^2$  short burst. Thus, niobium radiators are far less vulnerable to beam weapons than are solar cells.

A host of other conditions can be estimated quickly from Figs. 8-18. For example, the polished aluminum skin of a missile might be melted by a short burst of  $50\text{ W/cm}^2$  in a particle beam; however, at least  $300\text{ J/cm}^2$  would be required in a laser beam because the aluminum would reflect over 85% of the incident light. Further, if the skin of the missile were plated with a thin film of silver or gold to give a reflectivity of 98 to 99%, the energy density required in the laser beam might be increased to as much as  $3000\text{ J/cm}^2$ .

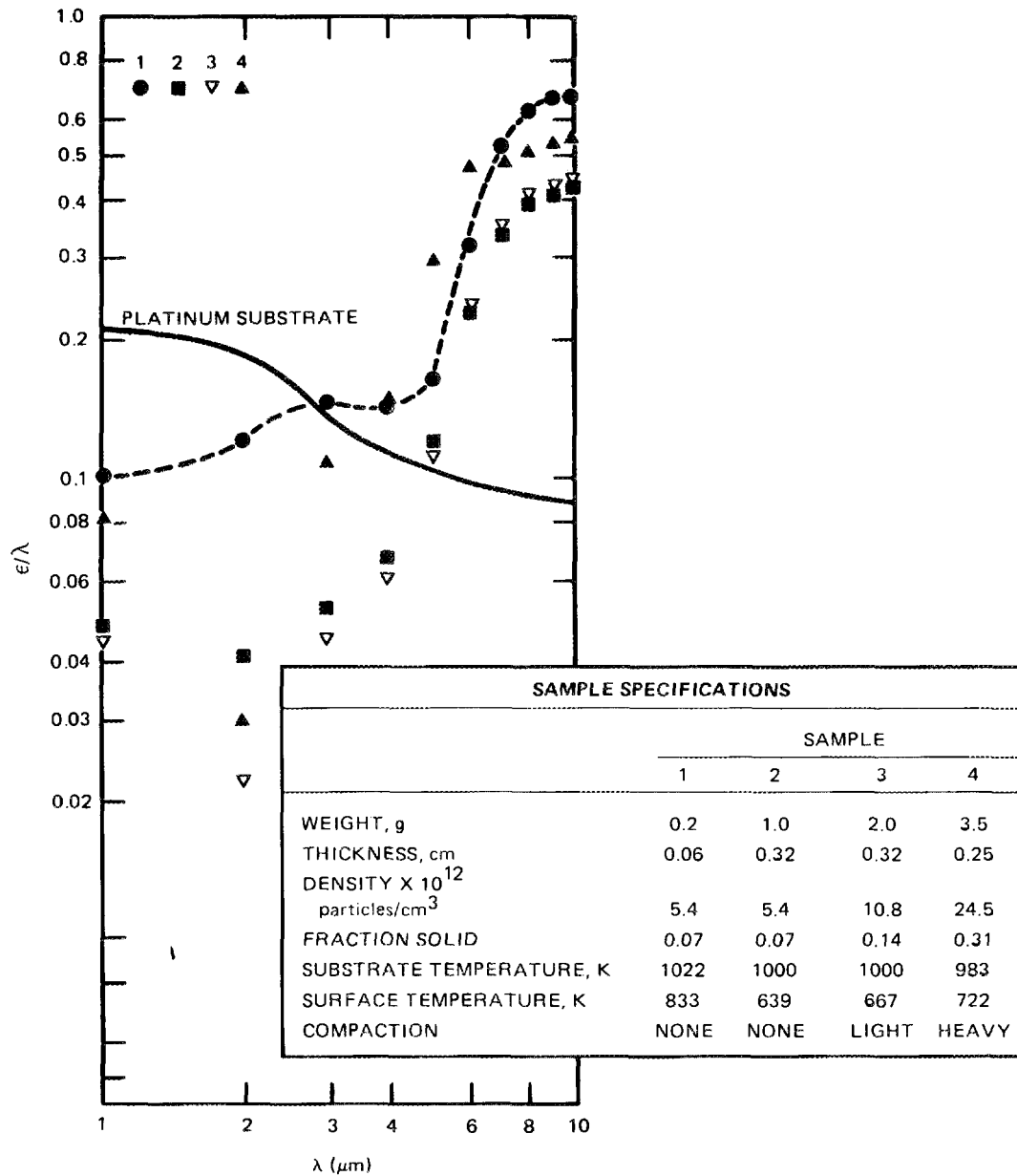


Fig. 27. Experimental values of apparent emittance of four samples of  $\text{Al}_2\text{O}_3$  powder. Source: J. B. Bergquam and R. A. Seban, "Spectral Radiation from Alumina Powder on a Metallic Substrate," *J. Heat Transfer* 94, 36-40 (February 1972), p. 37.

A number of particular cases were examined in the above presentation to illustrate the applicability of these tables and charts. Of the many other cases of interest, a few deserve mention here. One of these is concerned with surface heating from short bursts in which the energy absorbed would not be sufficient even to melt a surface layer, but the temperature gradient through the skin of an ascending missile, for example, might cause sufficient distortion that a thin, cylindrical shell in compression would buckle and lead to a catastrophic failure of the spacecraft. Similarly, explosive vaporization from a small area near one end of a missile might cause it to tumble so that it would reenter in an unfavorable orientation and burn up. Examples of this sort are too dependent on the particular design to treat here, but this sort of vulnerability should not be overlooked.

A plastic film can be vaporized with a much smaller energy pulse than a metal. Thus, any painted surface, as well as any plastic component, would be very vulnerable to even low-energy bursts of radiation. Not only is the energy per gram required for vaporization small, but also the thermal conductivity of plastics is lower than for metals by a factor of 10 to 100, and the velocity of sound in plastics is about one-third of that in metals.

Spacecraft may be damaged by radiation from nuclear explosions over 100 km away. The charts and tables presented here should be helpful in assessing these effects.

## 5.2 Swarms of Birdshot

Hostile action could take the form of swarms of birdshot released in the same orbit but in a retrograde direction to maximize the energy released on impact. The writer has treated the basic problem in a companion report on damage to spacecraft from meteoroids;<sup>25</sup> only the special problems posed by the threat of enemy action are treated here.

The crux of the threat lies in the enormous amount of kinetic energy per gram of projectile implicit in the relative velocity of such missiles:  $\sim 100,000$  J/g, or nearly 30 times the energy content of a high

explosive. Further, the impact velocity is well above the velocity of sound in structural metals so that potentially destructive shock waves are produced by an impact. In this hypervelocity regime (i.e., where the impact velocity exceeds the velocity of sound in the target), the penetration mechanism is quite different from that conventionally experienced; a hemispherical crater is formed that has a diameter several times that of the projectile, instead of the usual cylindrical hole that is essentially the diameter of the projectile. Furthermore, unless the target thickness is substantially greater than the depth of the crater, the shock wave reflected from the rear face of the target plate will induce such high tensile stresses in the vicinity of the rear face that a chunk will spall from the back of the plate. This will leave a ragged, relatively shallow crater commonly larger in diameter than the smooth, hemispherical crater on the front face. Thus, to ensure that a wall will not be penetrated, the wall thickness must be substantially greater than the depth of the impact crater in a thick target. A widely used empirical equation giving the wall thickness for incipient penetration has been evolved from extensive hypervelocity test work:<sup>25,26</sup>

$$t = K_1 m^{0.352} \rho^{0.167} V^{0.875} ,$$

where

- t = wall thickness, cm;
- $K_1$  = a constant dependent on the target material;
- m = mass of projectile, g;
- $\rho$  = density of the projectile, g/cm<sup>3</sup>;
- V = impact velocity, m/s.

Values given in Ref. 26 for  $K_1$  are 0.57 for 2024-T3 aluminum, 0.32 for AISI 316 stainless steel, 0.34 for Nb-1% Zr, and 0.80 for the Mg-Li alloy LA 141-A (see Refs. 27 and 28 for further details). This equation was used to prepare Fig. 28 to facilitate estimates of the armor required for protecting spacecraft against swarms of birdshot. The chart was drawn for aluminum targets struck by steel projectiles; relatively small correction factors tabulated on the chart equation can be applied easily to give estimates for other target and projectile materials.

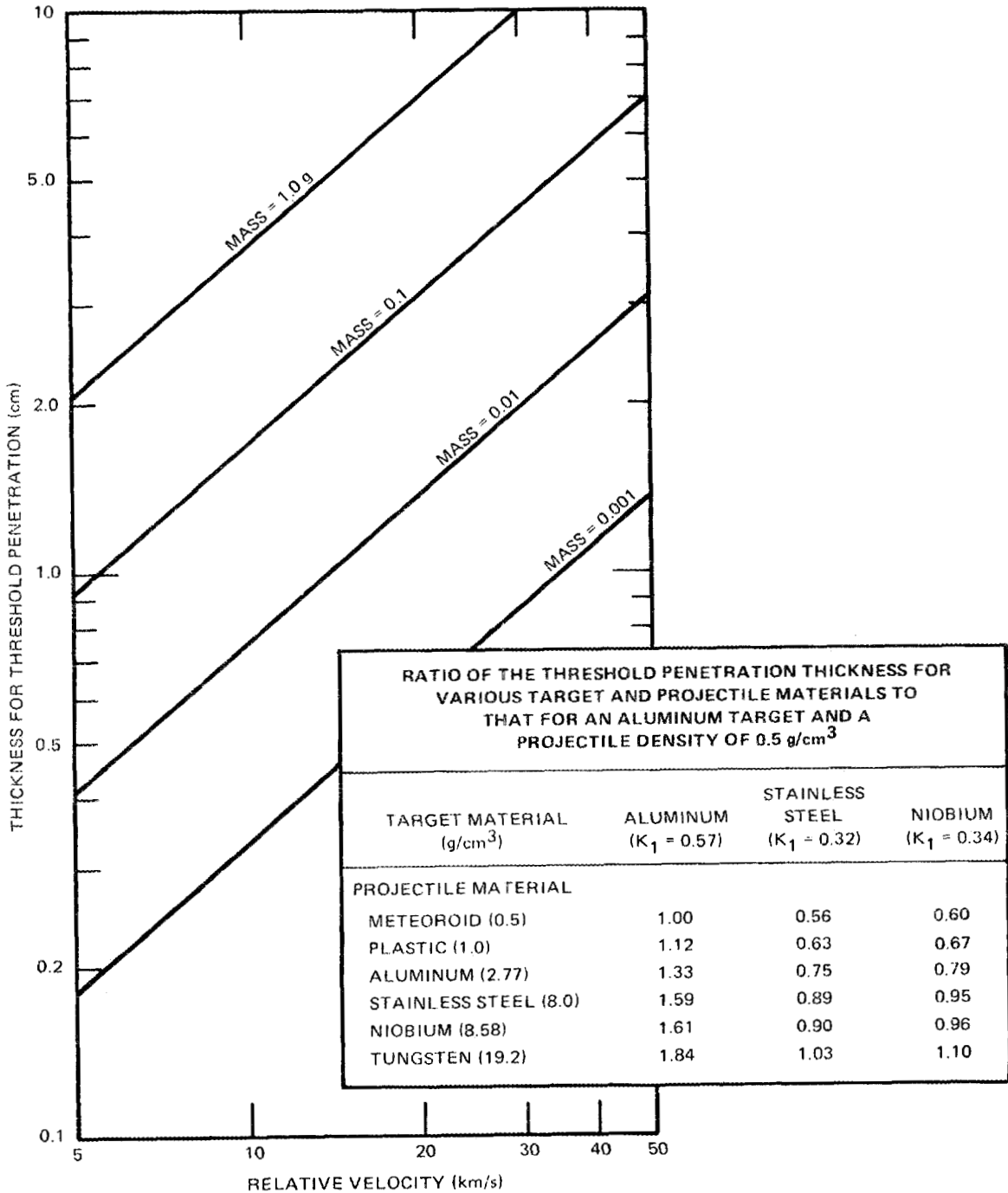


Fig. 28. Effect of relative impact velocity on thickness of aluminum 2024-T3 required for threshold penetration by meteoroids with density of 0.5 g/cm<sup>3</sup>. Source: R. Madden, *Ballistic Limit of Double-Walled Meteoroid Bumper Systems*, NASA Technical Note D-3916, National Aeronautics and Space Administration, Washington, D.C., April 1967.

It has been found that a bumper mounted at a substantial stand-off distance provides an attractive method for protecting a surface from hypervelocity projectiles. The energy release associated with the impact of a projectile on even a thin sheet is so great that it serves to shatter or vaporize both the slug punched from the sheet and the projectile. The fairly detailed treatment of this problem in Ref. 25 will not be repeated here, but Fig. 29 has been taken from Ref. 25 to show the effects of the principal parameters, particularly the kinetic energy in the projectile that is converted into heat by such an inelastic collision. The network of lines at the left shows the resulting temperature rise in the projectile; that at the right shows the corresponding temperature rise for the slug punched from the bumper. It must be emphasized that the calculations for this chart were made by assuming an inelastic collision in which one-half of the kinetic energy converted to heat appears in the projectile and one-half in the slug punched from the bumper. Unfortunately, available test data are limited, and there are some differences of opinion on their interpretation; however, Fig. 29 seems to be reasonably consistent with the information at hand.

A number of points must be kept in mind in using Fig. 29. In the first place, in the lower impact velocity region the projectile will only be fragmented, not melted or vaporized, and the penetrating power of the fragments will be independent of the stand-off distance of the bumper from the surface it protects. At higher velocities where the projectile would be vaporized, however, the cloud of vapor will expand as it travels beyond the bumper, and the pressure developed when it hits the target will fall off with an increase in the separation distance between the bumper and the target. Another important implication of Fig. 29 is that a plastic bumper should be superior to a metallic bumper in the low-impact velocity regime because much less energy is required to vaporize the plastic and provide a rapidly expanding cloud of vapor to disperse the cloud of fragments from the projectile. Perhaps even more important, the use of a plastic bumper will avoid the possibility that large fragments torn from the edges of the hole in the bumper itself may be a more serious threat to the target than fragments of the projectile. Note that for projectile velocities just below the hypervelocity

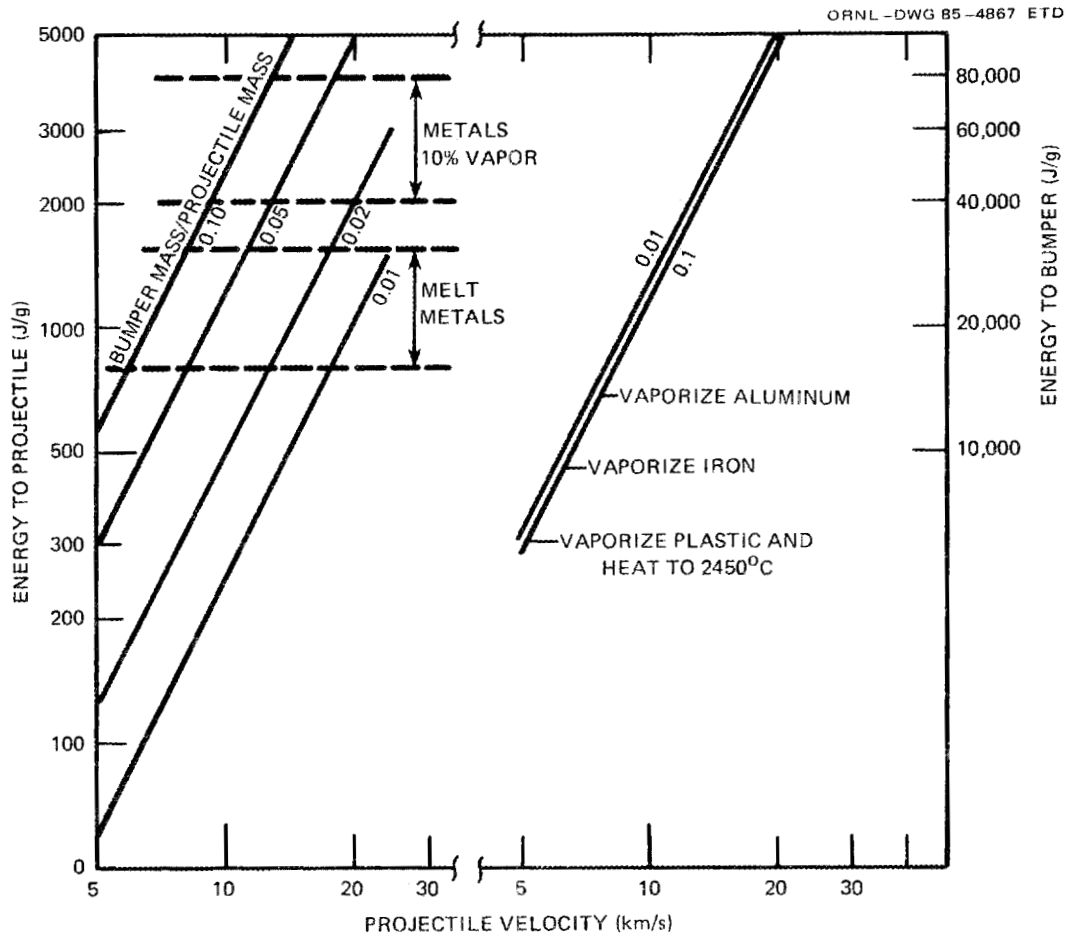


Fig. 29. Effect of impact velocity on residual energy appearing as heat in projectile and debris from bumper, assuming inelastic collision and equal division of heat between the two. Parameter is ratio of mass ejected from bumper to that of incident projectile. Source: A. P. Fraas, *Protection of Spacecraft from Meteoroids and Orbital Debris*, ORNL/TM-9904, Martin Marietta Energy Systems, Inc., Oak Ridge Natl. Lab., February 1986, p. 30.

regime, the penetration is actually substantially greater than at velocities above the velocity of sound in the target because of differences in the mechanics of material deformation in the course of the impact. Thus, in further test programs particular attention should be given to the use of plastic bumpers to provide a more comprehensive set of data for design purposes. Also, more data must be obtained at impact velocities around 15 km/s (most of the experiments to date have been with velocities below 10 km/s).<sup>25,27</sup> Such experiments will be difficult to run because of the truly formidable problems involved in getting projectile velocities above 12 km/s in controlled experiments. This has yet to be accomplished with projectiles of the size and shape required for the region of interest here.

One of the most convincing experiments designed to investigate the efficacy of bumpers was carried out by NASA in space using Explorer 46. The results of this experiment with a bumper designed to protect against meteoroids showed that for a given level of protection, the weight required for the bumper system was lower by a factor of 6.9 than the armor required without a bumper.<sup>28</sup>

An even greater weight savings appears possible by using a somewhat different design approach worked out at the Ballistics Research Lab, Aberdeen, Maryland. A set of charts from that work is presented in Ref. 29 and has been reproduced in Ref. 25. One chart of this set that is particularly likely to prove useful to readers of this report is included here as Fig. 30.

### 5.3 Shielding Spacecraft from Hostile Action

An interesting possibility for protecting spacecraft from enemy weapons is the use of a large disk of thin, plastic sheet faced with a highly reflective film of aluminum, silver, or gold, depending on the wavelength of the laser beams with which it might be threatened (see Fig. 5). This disk would normally be deployed between the spacecraft and the earth to protect the satellite from a surprise attack by beam weapons fired from the earth's surface. In the event that radar

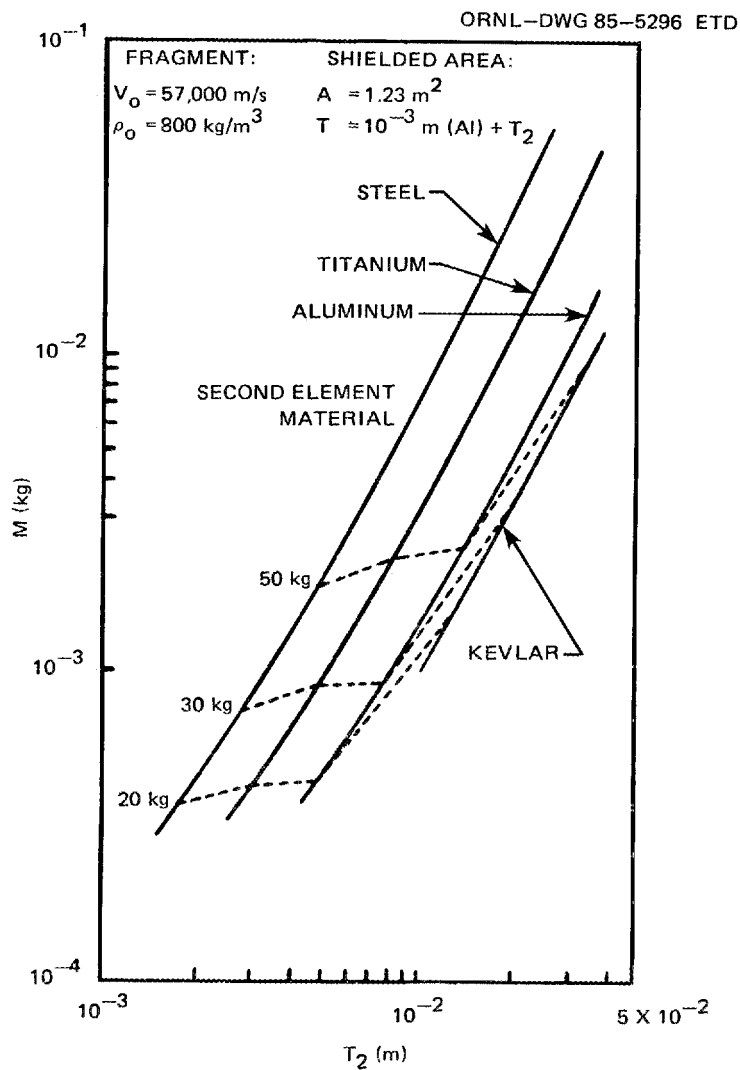


Fig. 30. Estimated mass  $M$  of comet fragment required for threshold penetration of various shield materials as function of shield thickness  $T_2$  for operation with a 1.0-mm-thick bumper of aluminum. Source: J. H. Klineke, Jr., "Probe Protection Against Cometary Meteoroid Attack," pp. 77-83 in *Proceedings of The Comet Halley Micrometeoroid Hazard Workshop*, Noordwijk, Netherlands, April 18-19, 1979, ESA-SP-153, European Space Agency.

scanning indicated that a swarm of birdshot was being launched in the spacecraft's orbit in the retrograde direction, the shield could be moved to a position in front of the spacecraft.

Another possibility that would provide simultaneous protection from both ground-based laser beams and swarms of birdshot is the use of a large plastic bubble surrounding the spacecraft. The side toward the ground could be faced with a reflective coating while the balance of the bubble could be left clear to permit the infrared emission from the radiator of the power plant to escape into space. A small fraction of the heat energy emitted from the radiator would be absorbed as it passed through the plastic film; therefore, the radius of the bubble must be large enough and its emissivity high enough to keep the equilibrium temperature of the plastic film to an acceptable level. As shown in the experimental data presented in Ref. 30, the absorption, reflectance, and emittance of plastic films vary in a highly complex fashion with the wavelength in the infrared region (see also Refs. 31 and 32). As a consequence, the design of a bubble of this type will be highly dependent on the radiator geometry and temperature of the particular power plant under consideration; thus, an attempt to prepare such a design was felt to be beyond the scope of this report. Note that this approach would also require sufficient shielding on the sides of the reactor to avoid serious damage to the plastic film from gamma and neutron radiation.

To keep the equilibrium temperature of the plastic at an acceptable level may require such a large bubble radius that the weight will be excessive. A somewhat similar but possibly lighter arrangement that might be used — a variation on the aluminum reflector troughs employed behind the radiator tubes in the ORNL designs of the 1960s — is indicated in Fig. 31 (see Refs. 33 and 34). In this case, the reflector would be a deep bowl of plastic film coated on both sides with a reflective layer of aluminum. The bowl contour would be an involute of revolution so that infrared rays from the radiator that strike its surface would be reflected out the open top and off into space. Note that this system has the advantage that the base material could be aluminum or a magnesium-lithium alloy rather than a transparent plastic so that it would not be subject to radiation damage.

ORNL-DWG 86-4767 ETD

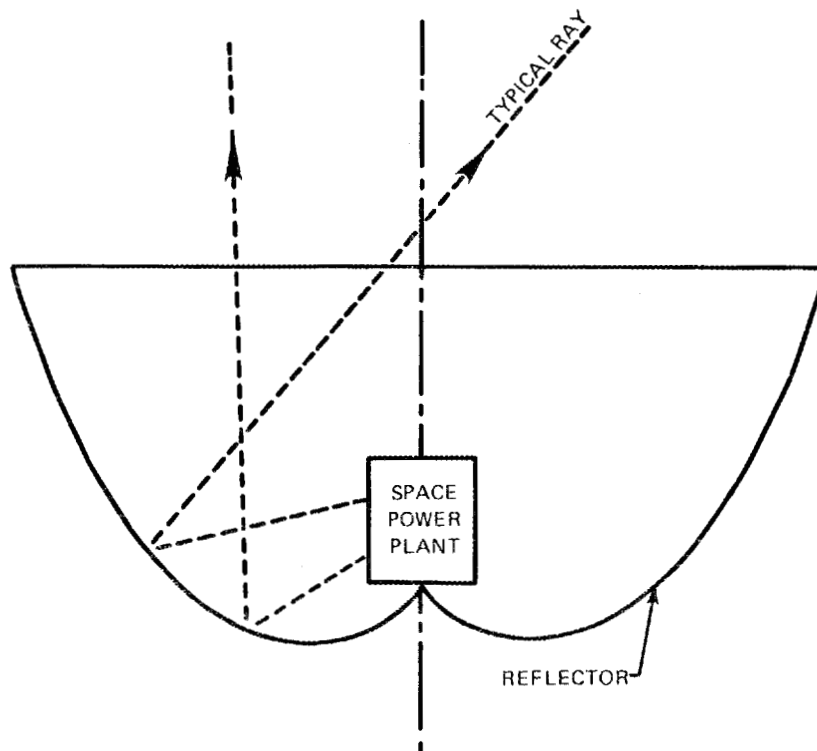


Fig. 31. Section through space power plant shielded from attack by lasers and buckshot with large reflector in form of surface of revolution about vertical axis. Energy emitted from power plant radiator in downward or lateral directions would be reflected out into space.

Any bumper system will be vulnerable to projectiles larger than those for which it was designed. Thus, the weight increment for the attacking system associated with increasing the projectile size may be less than the weight increment involved in increasing the thickness of the bumper to counter the more severe threat. The situation will depend heavily on both the precision with which the swarm of birdshot can be aimed and the length of time that the enemy may be willing to wait before a damaging collision is likely to occur. In view of this, for a spacecraft with a nuclear electric power supply, a much lighter approach to the birdshot problem may be the use of an ion jet to take evasive action, possibly by propelling the spacecraft on a random walk. This approach moves the problem of defensive-system evaluation from the area of power-plant design to spacecraft mission planning, again beyond the scope of this report.

## REFERENCES

1. *Proceedings on the Workshop on Dynamic Power Systems for Space Stations*, NASA Lyndon B. Johnson Space Center, Jan. 31 to Feb. 2, 1984.
2. A. P. Fraas and A. S. Thompson, *ORNL Fusion Power Demonstration Study: Fluid Flow, Heat Transfer, and Stress Analysis Considerations in the Design of Blankets for Thermonuclear Reactors*, ORNL/TM-5960, Union Carbide Corp. Nuclear Div., Oak Ridge Natl. Lab., February 1978.
3. H. A. Nyenhuis, "Practical Applications of Electron Beam Welding and Milling," pp. 124-143 in *Proceedings of Electron Beam Symposium, 8th Annual Meeting*, Allied General Corp., Medford, Mass., April 1964, p. 124.
4. N. Rykalin et al., *Laser Machining and Welding*, tr. O. Glebov, Pergamon Press, New York, 1978.
5. F. F. Y. Wang, *Laser Materials Processing, Materials Processing Theory and Practice*, vol. 3, North Holland Publishing Co., Amsterdam, 1983.
6. K. A. Brueckner, pp.155-236 in *Some Aspects of Compression and Heating, Course on Pulsed Fusion Reactors, International School of Reactor Technology*, Erice, Sicily, Sept. 9-15, 1974, Pergamon Press, New York, 1975.
7. R. E. Bolz and G. L. Tuve, eds., *Handbook of Tables for Applied Engineering Science*, 2d ed., CRC Press, Cleveland, 1973, pp. 207-17.
8. G. P. Harnwell, *Principles of Electricity and Electromagnetism*, McGraw-Hill Book Co., Inc., New York, 1949, p. 585.
9. J. W. Victoreen, "The Calculation of X-ray Mass Absorption Coefficients in Practice," *J. Appl. Phys.* 20, 1141-47 (December 1949).
10. *Handbook of Chemistry and Physics*, 40th ed., CRC Press, Cleveland, 1959.
11. *1980 Calendar and Reference Book*, Westinghouse Fusion Power Systems, Pittsburgh, 1980.
12. Y. S. Touloukian and E. H. Buyco, *Thermophysical Properties of Matter*, IFI/Plenum, New York, 1970.
13. L. B. Pankratz, *Thermodynamic Properties of Elements and Oxides*, Bureau of Mines Bulletin 672, Washington, D.C., 1982.

14. O. Kubaschewski and C. B. Alcock, *Metallurgical Thermal Chemistry*, 5th ed., Pergamon Press, New York, 1979.
15. Battelle Memorial Institute, comp., *Refractory Ceramics for Aerospace, A Materials Selection Handbook*, The American Ceramics Society, Columbus, Ohio, 1964.
16. M. Jakob, *Heat Transfer*, John Wiley & Sons, Inc., New York, 1950, p. 256.
17. M. Gross, *Explosive Impulse Calculations*, Report AFRPL-TR-71-2, Contract No. F 04611-69-C-0062, Air Force Rocket Propulsion Laboratory, Edwards Air Force Base, Calif., November 1970.
18. A. N. Pirri, "Theory of Momentum Transfer to a Surface with a High-Power Laser," *Phys. Fluids* 16, 1435-40 (September 1973).
19. D. B. Nichols and R. B. Hall, "Thermal Coupling of 2.8  $\mu\text{m}$  Laser Radiation to Metal Targets," *AIAA J.* 18(4), 476-78 (April 1980).
20. L. R. Hettele et al., "Mechanical Response and Thermal Coupling of Metallic Targets to High-Intensity 1.06  $\mu\text{m}$  Laser Radiation," *J. Appl. Phys.* 47(4), 1415-21 (April 1976).
21. N. Ferriter et al., "Laser Beam Optimization for Momentum Transfer by Laser-Supported Detonation Waves," *AIAA J.* 15(11), 1597-603 (November 1977).
22. J. J. Keyes and A. I. Krakoviak, "High Frequency Surface Thermal Fatigue Cycling of Inconel at 1406°F," *Nucl. Sci. Eng.* 9(4), 462-66 (April 1961).
23. A. P. Fraas, *Engineering Evaluation of Energy Systems*, McGraw-Hill Book Co., Inc., New York, 1982, pp. 161-64.
24. J. B. Bergquam and R. A. Seban, "Spectral Radiation from Alumina Powder on a Metallic Substrate," *American Society of Mechanical Engineers Transactions, J. Heat Transfer* 94, 36-40 (February 1972).
25. A. P. Fraas, *Protection of Spacecraft from Meteoroids and Orbital Debris*, ORNL/TM-9904, Martin Marietta Energy Systems, Inc., Oak Ridge Natl. Lab., February 1986.
26. *Meteoroid Damage Assessment*, NASA SP-8042, National Aeronautics and Space Administration, Washington, D.C., May 1970.
27. R. Madden, *Ballistic Limit of Double-Walled Meteoroid Bumper Systems*, NASA Technical Note D-3916, National Aeronautics and Space Administration, Washington, D.C., April 1967.

28. D. H. Humes, *Meteoroid Bumper Experiment on Explorer 46*, NASA Technical Paper 1879, National Aeronautics and Space Administration, Washington, D.C., July 1981.
29. J. H. Kineke, Jr., "Probe Protection Against Cometary Meteoroid Attack," pp. 77-83 in *Proceedings of the Comet Halley Micrometeoroid Hazard Workshop*, Noordwijk, Netherlands, April 18-19, 1979, ESA-SP-153, European Space Agency.
30. G. L. Tien et al., "Infrared Radiation of Thin Plastic Films," American Society of Mechanical Engineers Transactions, *J. Heat Transfer* 94, 41-45 (February 1972).
31. H. R. Carlon, "Refractive Indices of Infrared-Transmitting Substrate Materials Calculated Using Standard Spectrophotometer Transmittance Curves," *Appl. Opt.* 8(6), 1179-82 (June 1969).
32. O. M. Sorokin et al., "Semi-Transparent, Vacuum-Tight Plastic Windows for the Vacuum Ultraviolet," *Sov. J. Opt. Technol. (USA)* 37(7), 143-44 (February 1970).
33. A. P. Fraas, "Design and Development Tests of Direct-Condensing Potassium Radiators," in *AIAA Specialists Conference on Rankine Space Power Systems*, vol. 1, USAEC Report CONF-651026, U.S. Atomic Energy Commission, Washington, D.C., October 1965.
34. R. S. Holcomb and F. E. Lynch, *Thermal Radiation Performance of a Finned Tube with a Reflector*, ORNL/TM-1613, Union Carbide Corp. Nuclear Div., Oak Ridge Natl. Lab., April 1967.



## Appendix A

TEMPERATURE DISTRIBUTIONS IN PLATES WITH SURFACES  
HEATED BY SHORT BURSTS OF RADIANT ENERGY

Jakob<sup>1</sup> has presented the solution to the problem of the temperature distribution in an infinitely thick plate of uniform properties, originally at a uniform temperature, whose surface is subjected to the sudden start of heating at a uniform rate, that is,

$$T - T_0 = \frac{2 Q \sqrt{\gamma t}}{k \tau} u \left( \frac{2}{\sqrt{\pi}} \int_0^u e^{-u^2} du + \frac{e^{-u^2}}{\pi u} - 1 \right), \quad (\text{A.1})$$

where

$T_0$  = initial temperature of the plate,

$T$  = temperature at a distance  $x$  from the surface of the plate at time  $t$ ,

$Q$  = energy input per unit of area in time  $\tau$ ,

$\tau$  = period of energy burst,

$x$  = distance from the surface,

$$u = \frac{x}{2\sqrt{\gamma t}},$$

$\gamma$  = thermal diffusivity =  $k/C_p \rho$

where

$k$  = thermal conductivity,

$c_p$  = heat capacity (constant pressure),

$\rho$  = density.

The solution of this equation at the end of the input period ( $t = \tau$ ) is

$$T - T_0 = \frac{2 Q}{\sqrt{k c_p \rho \tau}} g(u) \quad (\text{A.2})$$

with the following tabulated values of  $g(u)$ .

$u = \frac{x}{2\sqrt{\gamma \tau}}$	$g(u)$
0.00	0.5642
0.10	0.4698
0.20	0.3866
0.30	0.3142
0.40	0.2522
0.50	0.1996
0.60	0.1559
0.70	0.1201
0.90	0.0682
1.00	0.0503
1.20	0.0261
1.50	0.0086
2.00	0.0009
3.00	0.0001

In this report Eq. (A.2) has been used to estimate the temperature distribution in a plate at the end of a short burst of radiant energy. The derivation assumes that the plate is relatively thick ( $>2\sqrt{\gamma\tau}$ ) and that the "constants"  $k$ ,  $c_p$ , and  $\rho$  may be averaged over the temperature range at a given distance from the surface. Calculations for estimating the total energy input for incipient vaporization use an effective heat capacity that is the quotient of the enthalpy difference and the temperature difference between the initial conditions and the point of incipient vaporization.

#### REFERENCE

1. M. Jakob, *Heat Transfer*, John Wiley & Sons, Inc., New York, 1950.

## Appendix B

## BLAST EFFECTS FROM RAPID VAPORIZATION FROM A SURFACE

The blast effects were estimated roughly by making a number of simplifying assumptions:

1. Evaporation from the surface occurs at a rate equal to the rate heat input divided by the heat of vaporization at the boiling point for 1 atm.
2. The energy input required to heat the surface to the boiling point is estimated using the methods of Appendix A with an effective value of heat capacity from the initial temperature through incipient vaporization.
3. The velocity of the vapor leaving the surface was taken as the sonic velocity for the vapor at the nominal boiling point at 1 atm. This was calculated by assuming that the vapor would be monatomic and by using the relation

$$V_s = \sqrt{g K R T} = 117\sqrt{T/M} ,$$

where  $V_s$  is in meters per second,  $T$  was taken as the atmospheric boiling point in degrees Kelvin, and  $M$  as the atomic weight.

4. The blast pressure from rapid vaporization is the reaction force per unit of area imparted by the momentum of the vapor leaving the surface. Thus,

$$P = F/A = V_s \frac{dm}{dt} = V_s \frac{(\text{mass vaporized/cm}^2)}{(\text{pulse time})} .$$

For the pressure in bars,

$$P = \frac{(\text{mass vaporized/cm}^2)(\text{sonic velocity, cm/s})}{(\text{pulse time, s}) 980 \times 10^5} .$$



Internal Distribution

- |        |                 |        |                               |
|--------|-----------------|--------|-------------------------------|
| 1.     | D. E. Bartine   | 31-40. | J. P. Nichols                 |
| 2.     | H. I. Bowers    | 41.    | D. U. O'Kain                  |
| 3.     | R. B. Burditt   | 42.    | M. Olszewski                  |
| 4.     | C. V. Chester   | 43.    | H. Postma                     |
| 5-6.   | R. H. Cooper    | 44.    | H. L. Roberts                 |
| 7.     | W. G. Craddick  | 45.    | R. T. Santoro                 |
| 8-17.  | A. P. Fraas     | 46.    | M. Siman-Tov                  |
| 18.    | F. P. Griffin   | 47.    | D. G. Thomas                  |
| 19.    | C. M. Haaland   | 48.    | H. E. Trammell                |
| 20.    | H. W. Hoffman   | 50.    | K. A. Williams                |
| 21.    | R. S. Holcomb   | 51.    | G. L. Yoder                   |
| 22.    | D. T. Ingersoll | 52.    | ORNL Patent Office            |
| 23.    | D. B. Lloyd     | 53.    | Central Research Section      |
| 24.    | S. R. McNeany   | 54.    | Document Reference Section    |
| 25-29. | J. C. Moyers    | 55-56. | Laboratory Records Department |
| 30.    | F. R. Mynatt    | 57.    | Laboratory Records (RC)       |

External Distribution

58. S. K. Bhattacharyya, Argonne National Laboratory, 9700 S. Cass Avenue, Argonne, IL 60439
59. R. Bohl, MS 560, Los Alamos National Laboratory, P.O. Box 1663, Los Alamos, NM 87545
60. R. G. Brengle, Rocketdyne Division, Rockwell International Corporation, 6633 Canoga Avenue, Canoga Park, CA 91303
61. B. G. Cour-Palais, NASA Johnson Space Center, Code SN3, Houston, TX 77058
62. C. M. Cox, Hanford Engineering Development Laboratory, P.O. Box 1970, Richland, WA 99352
63. L. Cropp, Sandia National Laboratories, P.O. Box 5800, Albuquerque, NM 87185
64. P. Dirkmaat, DOE-ID, 550 Second Street, Idaho Falls, ID 83274
65. R. E. English, NASA Lewis Research Center, MS 501-15, 21000 Brookpark Road, Cleveland, OH 44135
66. D. H. Humes, NASA Langley Research Center, MS 160, Hampton, VA 23665-5225
67. D. J. Kessler, NASA Johnson Space Center, Code SN3, Houston, TX 77058
68. E. U. Khan, U.S. Dept. of Energy, NE-54, Germantown, Washington, D.C. 20545
69. J. H. Kineke, Jr., Ballistics Research Laboratory, SLCBR-TB/W, Aberdeen Proving Ground, Aberdeen, MD 21005-5066.
70. J. H. Lee, Jr., Sandia National Laboratory, Dept. 6430A, P.O. Box 5800, Albuquerque, NM 87185

71. J. Loria, NASA Headquarters, 400 Maryland Avenue SW, Washington, D.C. 20546
72. E. T. Mahefkey, Jr., Aero Propulsion Laboratory (POOC-5), U.S. Air Force Wright Aeronautical Laboratories, Wright-Patterson Air Force Base, OH 45433
73. J. R. Powell, Brookhaven National Laboratory, Associated Universities, Inc., Upton, NY 11973
74. R. E. Rice, EG&G Idaho, 1955 Freemont, Idaho Falls, ID 83401
75. J. M. Smith, NASA Lewis Research Center, MS 500-202, Building 4013, 21000 Brookpark Road, Cleveland, OH 44135
76. R. J. Sovie, NASA Lewis Research Center, MS 500-202, Building 4013, 21000 Brookpark Road, Cleveland, OH 44135
77. R. Verga, Strategic Defense Initiative/Director of Energy, The Pentagon, Washington, D.C. 20301-7100
78. E. J. Wahlquist, U.S. Dept. of Energy, NE-54, Germantown, Washington, D.C. 20545
79. C. E. Walter, Lawrence Livermore National Laboratory, University of California, P.O. Box 808, Livermore, CA 94550
80. J. Wetch, Space Power Inc., 253 Humboldt Court, Sunnyvale, CA 94089
81. R. D. Widrig, Pacific Northwest Laboratory, Battelle Boulevard, Richland, WA 99532
82. G. R. Woodcock, Boeing Aerospace Company, Post Office Box 1470, Huntsville, AL 35807
83. R. Wylie, Strategic Defense Initiative/Director of Energy, The Pentagon, Washington, D.C. 20301-7100
84. H. R. Zweig, Energy Technology Engineering Center, Rocketdyne Division, Rockwell International Corp., P.O. Box 1449, Canoga Park, CA 91304
85. Office of Assistant Manager for Energy, Research and Development, DOE-Oak Ridge Operations, Oak Ridge, TN 37831
- 86-115. Office of Scientific and Technical Information, P.O. Box 62, Oak Ridge, TN 37831